LA-UR-12-26037
Approved for public release; distribution is unlimited.

Title: Residual a posteriori error estimation of a mimetic/virtual element method

Author(s): Manzini, Gianmarco
Beirao da Veiga, Lourenco

Intended for: Report

RESIDUAL A-POSTERIORI ERROR ESTIMATION OF A MIMETIC/VIRTUAL ELEMENT METHOD

LOURENÇO BEIRÃO DA VEIGA * AND GIANMARCO MANZINI †

Abstract. A posteriori error estimation and adaptivity are very useful in the context of the mimetic finite difference method due to the flexibility of the meshes to which this family of numerical schemes can be applied. Nevertheless, developing error estimators for mimetic methods is not a straightforward task due to the lack of knowledge of the basis functions. This issue is tackled by the virtual element method recently introduced in [4], which can be interpreted as a Galerkin reformulation of the mimetic finite difference method. In the new virtual element setting, we develop a residual based a posteriori error estimator that immediately applies to its mimetic counterpart. For such estimator we prove the reliability and we show the numerical performance when it is combined with an adaptive strategy for the mesh refinement. For the lowest-regular approximation we also developed an *hp*-adaptive strategy based on the comparison between the numerical solution on a base mesh and on a reference mesh.

Key words. a posteriori error estimation, virtual element method, mimetic discretization method, polygonal mesh, high-order scheme

1. Introduction. The Virtual Element Method (VEM) is a generalization of the Finite Element (FE) method [13, 17, 11, 22, 10] that achieves a higher degree of flexibility in terms of meshes and properties of the scheme by avoiding an explicit construction of the discrete shape functions. For its implementation, the method makes use of an approximated bilinear form $\mathcal{A}_h$ that mimics the original bilinear form $\mathcal{A}$ and satisfies precise conditions of stability and consistency to guarantee well-posedness and convergence. VEM has been introduced in [4] for the Poisson problem and then extended to the compressible and almost incompressible elasticity problem in [5]. This family of schemes has a very deep relation with the Mimetic Finite Difference (MFD) method, for which we refer the reader to [14, 16, 3, 12, 6]. The connection is so strong that VEM can be interpreted as a Galerkin re-formulation of the MFD method, and most of the mimetic schemes of the recent literature can be easily reformulated in the virtual element setting. Furthermore, such reformulation provides an elegant formalism and a better understanding of the mimetic discretizations.

Due to the large flexibility of the meshes to which the mimetic and the virtual element methods are applied, mesh adaptivity becomes an appealing feature as mesh refinement and de-refinement strategies can be implemented very efficiently. Hanging nodes can be introduced in the mesh without spreading the refined zones in order to guarantee the mesh conformity. Polygonal cells with very general shapes are admissible thus allowing us to adopt simple mesh coarsening algorithms.

There is a very large literature about a posteriori error estimations for finite elements, see for instance [26, 1]. Unfortunately, for mimetic and virtual element methods the a posteriori error analysis is more involved as there is no explicit knowledge of the basis functions inside the elements and to devise residual-based error estimators, which are among the most popular ones in FE analysis, is particularly difficult. This is reflected by the fact that in the mimetic literature there are very few papers devoted to the a-posteriori analysis. In [3, 7], the authors circumvent the difficulty due to the absence of the shape functions by introducing a post-processed pressure

[1]Dipartimento di Matematica F. Enriques, Università degli Studi di Milano, via Saldini 50, 20133 Milano, Italy, e-mail: lourenco.beirao@unimi.it

[2]Los Alamos National Laboratory, Theoretical Division, Group T-5, MS B284, Los Alamos, NM-87545, USA e-mail: gmanzini@lanl.gov

solution that is used in the computation of the residual. This approach is successful for the MFD method of [14, 8] for the diffusion problem in mixed form. Regarding the diffusion problem in primal form, a hierarchical estimator, which does not require any evaluation of residuals, is proposed in [2]. This estimator is suitable to the low-order method presented in [12], but a direct extension to the arbitrary-order mimetic method in [6], which is based on variable polynomial degree, may be cumbersome.

In this work, we develop a residual-based estimator for the virtual element method for diffusion problems in primal form presented in [9]. This family of schemes are characterized by a general polynomial degree of accuracy m and a general regularity index $\alpha \in \mathbb{N}$, i.e., the numerical approximations they provide belong to $C^\alpha(\Omega)$. Although the shape functions inside the elements are unknown, when $\alpha = 1$ it is possible to derive a residual-based error estimator by exploiting some specific characteristics of the virtual method. Such estimator is then sum of local terms, each one of which being composed by three distinct parts associated with the residual, the approximation of the loading term and the approximation of the bilinear form.

For the low-regular cases, i.e., $\alpha = 0$ and $m \geq 1$, we also present an hp-refinement strategy, where the error estimation makes use of a reference solution. This method is adapted from the hp-adaptive strategy developed by Demkowicz and collaborators, see, e.g. [19, 20, 24, 25], and the refinement technique of Melenk and Wohlmuth [23]. Refinement decisions are taken by comparing the actual solution with a reference solution, and proceeds by first computing a reference solution on a uniformly refined mesh with a polynomial degree which is higher than 1, and, then, by deciding which cells display the bigger error, i.e., so for which cells we must take the refinement and if this refinement must be of h or p type.

The paper is organized as follows. In Section 2 we present the mathematical model. In Section 3 we briefly review the method in [9] for $\alpha = 1$ and a general positive integer m. In Section 4 we introduce the a posteriori error estimator and we prove that it bounds the energy error from above up to a uniform constant. In Section 5 we show the performance of such estimator when it is combined with an adaptive strategy in the resolution of a set of model problems. Finally, in Section 6 we offer our final remarks and discusses the open issues for future work.

2. The mathematical model. Let us consider the Poisson problem for the scalar solution field u given by

$$-\Delta u = f \quad \text{in} \quad \Omega, \tag{2.1}$$

$$u = g \quad \text{on} \quad \partial\Omega, \tag{2.2}$$

where Ω is a bounded, open, polygonal subset of $\mathbb{R}^2$, f in $L^2(\Omega)$ is the forcing term, and g in $H^{\frac{1}{2}}(\partial\Omega)$ is the boundary datum. To ease the theoretical presentation, we consider the case of homogeneous Dirichlet boundary conditions, i.e., $g = 0$ on $\partial\Omega$, while the more general case of non-homogeneous boundary conditions is investigated in the section of numerical experiments.

Throughout the paper, we follow the usual notation for Sobolev spaces, inner products and norms, see, e.g., [18]. For an open bounded domain $\mathcal{D}$, we use the notation $\|\cdot\|_{s,\mathcal{D}}$ and $|\cdot|_{s,\mathcal{D}}$ for the norm and the seminorm in the Sobolev space $H^s(\mathcal{D})$, and the notation $(\cdot,\cdot)_{0,\mathcal{D}}$ for the $L^2(\mathcal{D})$ inner product. The subscript $\mathcal{D}$ is generally omitted when $\mathcal{D}$ is the computational domain Ω. We also represent the set of polynomials defined on P that have degree less than or equal to the integer j by $\mathbb{P}_j(\mathsf{P})$ and the $L^2(\mathcal{D})$ orthogonal projection onto $\mathbb{P}_j(\mathcal{D})$ by $\pi_j^{\mathcal{D}}$.

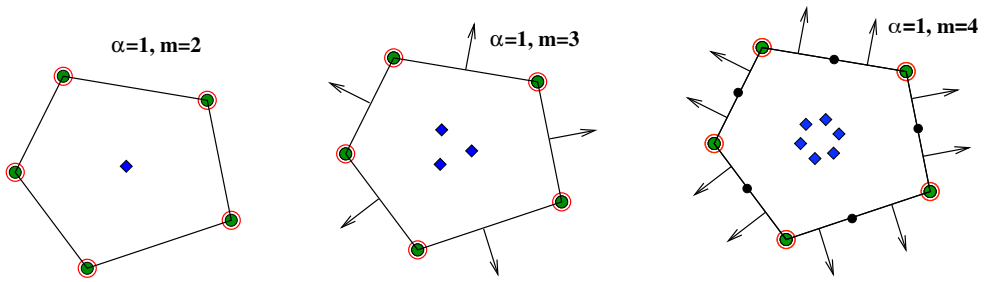

FIG. 3.1. *The degrees of freedom for $\alpha = 1$ and $m = 2, 3, 4$. The symbols shown in the plots represent the nodal values (dots) at the mesh vertices and edges, the first-order derivatives at the vertices (circles), the first-order normal derivatives at the mesh edges (arrows), and the internal moments (squares).*

Let us now consider the functional space $H^1_0(\Omega) = \{v \in H^1(\Omega),\ v_{|\partial\Omega} = 0\}$. Problem (2.1)-(2.2) can be restated in the variational form:

find $u \in H^1_0(\Omega)$ such that

$$\mathcal{A}\big(u, v\big) = \big(f, v\big) \qquad \forall v \in H^1_0(\Omega), \tag{2.3}$$

where

$$\mathcal{A}\big(u, v\big) = \int_\Omega \nabla u \cdot \nabla v \, dV \quad \text{and} \quad \big(f, v\big) = \int_\Omega f v \, dV. \tag{2.4}$$

The bilinear form $\mathcal{A}$ is continuous and coercive and the linear functional $\big(f, \cdot\big)$ is continuous, thus implying the well-posedness of problem (2.3), i.e., existence and uniqueness of the weak solution [21].

3. A C^1 Virtual Element Method. Let $\{\Omega_h\}_h$ be a sequence of decompositions of Ω into elements P labeled by the mesh size parameter h. For the moment, we assume that each decomposition Ω_h is a finite number of *simple polygons*, i.e., open simply connected subsets of Ω whose boundary is a non-intersecting line composed by a finite number of straight line segments. The precise assumption about the mesh regularity, which is required to perform the convergence analysis of the method, will be given in subsection 3.7, see Assumption 3.2.

Let us consider the virtual element method of [9]. This method defines a family of mimetic schemes for each couple of integers (α, m), where $\alpha \geq 0$ is the *regularity index* and $m \geq \alpha + 1$ is the *consistency index*. All these schemes provide a numerical approximation to the solution of (2.3) that is C^α regular and $\mathcal{O}(h^m)$ accurate in the energy norm. Let us focus on the case $\alpha = 1$ and consider the family of mimetic schemes associated with each integer number $m \geq 2$. In the next subsections, for every h we will construct a finite dimensional space $V_h \subset H^1_0(\Omega)$, a family of bilinear forms $\mathcal{A}_h : V_h \times V_h \to \mathbb{R}$ and a loading term $\big(f_h, v_h\big)_h$, which, respectively, approximate the bilinear form $\mathcal{A}$ and the linear functional $\big(f, v\big)$ in (2.4). The VEM method for the discretization of (2.3) reads as:

find $u_h \in V_h$ such that:

$$\mathcal{A}_h\big(u_h, v_h\big) = \big(f_h, v_h\big) \qquad \forall\, v_h \in V_h. \tag{3.1}$$

3.1. Local discrete spaces. We denote a generic mesh vertex by v, a generic mesh edge by e and its length by $|\mathsf{e}|$, the area of polygon P by $|\mathsf{P}|$ and its boundary by $\partial\mathsf{P}$. The orientation of each edge e is reflected by the unit vector $\mathbf{n}_\mathsf{e}$, which is orthogonal to e and fixed once and for all. For any polygon P and any edge e of $\partial\mathsf{P}$, we define the unit normal vector $\mathbf{n}_{\mathsf{P},\mathsf{e}}$ that points out of P. We denote the set of mesh vertices by $\mathcal{V}$ and the set of mesh edges by $\mathcal{E}$.

For any integer $s \geq 0$ and any polygonal cell P, we consider the functional space of piecewise polynomials of degree s defined on the boundary $\partial\mathsf{P}$:

$$\mathbb{B}_s(\partial\mathsf{P}) := \left\{ v \in L^2(\partial\mathsf{P}) \,:\, v_{|\mathsf{e}} \in \mathbb{P}_s(\mathsf{e}),\, \forall \mathsf{e} \in \partial\mathsf{P} \right\}.$$

Let u introduce the integers $\alpha_0 := \max\{3, m\}$ and $\alpha_1 := \max\{1, m-1\}$. For any index $m \geq 2$, we consider the local finite element space associated with the polygonal cell P given by:

$$V_{h|\mathsf{P}} = \Bigg\{ v \in H^2(\mathsf{P}) \text{ with } \Delta^2 v \in \mathbb{P}_{m-2}(\mathsf{P}) \text{ s. t. } v_{|\partial\mathsf{P}} \in \mathbb{B}_{\alpha_0}, \tag{3.2}$$

$$\frac{\partial v}{\partial n}\Big|_{\partial\mathsf{P}} \in \mathbb{B}_{\alpha_1}(\partial\mathsf{P}), \nabla v_{|\partial\mathsf{P}} \in C^0(\partial\mathsf{P}) \Bigg\}, \tag{3.3}$$

with the convention that $\mathbb{P}_{-1}(\mathsf{P}) = \{0\}$ and where Δ^2 represents the biharmonic operator.

For example, for $m = 2$ we obtain the finite element space of functions in $H^2(\mathsf{P})$ such that:

- the trace on the boundary of P is continuous and is a piecewise polynomial of degree $\alpha_0 = 3$;
- the gradient on the boundary is continuous and the normal derivative on each edge is a polynomial of degree $\alpha_1 = 1$;
- in the interior of P, these functions satisfies the bi-harmonic equation $\Delta^2 v = p$ for some $p \in \mathbb{R}$.

REMARK 3.1. *The local space $V_{h|\mathsf{P}}$ in* (3.3) *is virtual in the sense that we do not need to build it explicitly for the practical implementation of the family of schemes here proposed.*

3.2. Local degrees of freedom. We distinguish three kinds of degrees of freedom that are associated with each polygonal cell P:

- $\mathcal{V}_\mathsf{P}^h$: *vertex* degrees of freedom of P;
- $\mathcal{E}_\mathsf{P}^h$: *edge* degrees of freedom of P;
- $\mathcal{P}_\mathsf{P}^h$: *interior* degrees of freedom of P.

In Figure 3.1 we show the degrees of freedom for a pentagonal element for $\alpha = 1$ and $m = 2, 3, 4$.

Vertex degrees of freedom. The vertex degrees of freedom of the function v associated with the vertex v are the values of v and of the partial derivatives of v evaluated at v.

Edge degrees of freedom. The edge degrees of freedom of the function v are the values of v and of the normal derivatives of v evaluated at certain distinct points along e. More precisely, on each open edge e we consider the set of $\mathcal{N}_0^m$ distinct nodes $\{\mathbf{x}_i^0\}_{i=1,\dots,\mathcal{N}_0^m}$ where $\mathcal{N}_0^m = \max(m-3, 0)$. The nodal degrees of freedom of v

associated with edge e are given by $v(\mathbf{x}_i^0)$, i.e., the values of v at $\mathbf{x}_i^0$. We also consider the set of $\mathcal{N}_1^m$ distinct nodes $\{\mathbf{x}_i^1\}_{i=1,\dots,\mathcal{N}_1^m}$ where $\mathcal{N}_1^m = \max(m-2,0)$. The normal derivative degrees of freedom of v associated with edge e are given by $\partial v(\mathbf{x}_i^1)/\partial n$, i.e., the normal derivative of v at $\mathbf{x}_i^1$. The points of the sets $\left\{\mathbf{x}_i^0\right\}_i$ and $\left\{\mathbf{x}_i^1\right\}_i$ can be uniformly spaced along e or chosen as the nodes of some integration rule like those provided by Gauss-Lobatto formulas, cf. [6].

Internal degrees of freedom. The internal degrees of freedom of the function v are the polynomial moments of v defined with respect to a certain basis of the local space of polynomials of degree up to $m-2$ on P. More precisely, let $\mathbf{s} = (s_1, s_2)$ with $s_1, s_2 \geq 0$ be a two-dimensional multi-index with the usual notation $|\mathbf{s}| := s_1 + s_2$ and $\mathbf{x}^{\mathbf{s}} = x_1^{s_1} x_2^{s_2}$ when $\mathbf{x} = (x_1, x_2)$. We consider the set of $m(m-1)/2$ monomials

$$\mathcal{M}_{m-2} = \left\{ \left(\frac{\mathbf{x} - \mathbf{x}_{\mathsf{P}}}{h_{\mathsf{P}}} \right)^{\mathbf{s}}, \, |\mathbf{s}| \leq m-2 \right\}, \tag{3.4}$$

which is a basis for the local polynomial space $\mathbb{P}_{m-2}(\mathsf{P})$. The *internal degrees of freedom* of a function v are the $m(m-1)/2$ moments:

$$\frac{1}{|\mathsf{P}|} \int_{\mathsf{P}} q(\mathbf{x})\, v(\mathbf{x})\, dV \qquad \forall q \in \mathcal{M}_{m-2}(\mathsf{P}).$$

REMARK 3.2. *On each edge e, the degrees of freedom $\mathcal{V}_{\mathsf{P}}^h$ plus $\mathcal{E}_{\mathsf{P}}^h$ uniquely determine a polynomial of degree α_0 on each edge e of P representing the function value, and a polynomial of degree α_1, representing the normal derivative. Thus, prescribing the degrees of freedom $\mathcal{V}_{\mathsf{P}}^h$ plus $\mathcal{E}_{\mathsf{P}}^h$ is equivalent to prescribing v and $\partial v/\partial n$ on $\partial\mathsf{P}$. On the other hand, prescribing the degrees of freedom $\mathcal{P}_{\mathsf{P}}^h$ is equivalent to prescribing the L^2-orthogonal projection $\pi_{m-2}^{\mathsf{P}}(v)$ onto the space of the polynomials of degree up to $m-2$ defined on P.*

REMARK 3.3. *As pointed out in [9], a better condition number of the stiffness matrix is obtained by scaling the nodal degrees of freedom by an opportune local mesh size factor.*

For the space $V_{h|\mathsf{P}}$ and the degrees of freedom $\mathcal{V}_{\mathsf{P}}^h$ plus $\mathcal{E}_{\mathsf{P}}^h$ plus $\mathcal{P}_{\mathsf{P}}^h$ we have the following *unisolvence result*, whose proof is found in [9].

PROPOSITION 3.1. *Let P be a simple polygon with $N_{\mathsf{P}}^{\mathcal{E}}$ edges, and the space $V_{h|\mathsf{P}}$ be generated by the monomials in* (3.3). *The degrees of freedom $\mathcal{V}_{\mathsf{P}}^h$ plus $\mathcal{E}_{\mathsf{P}}^h$ plus $\mathcal{P}_{\mathsf{P}}^h$ are unisolvent for $V_{h|\mathsf{P}}$.*

3.3. Construction of the finite element space V_h. We can now design V_h, the *virtual element space* on the whole domain Ω. For every decomposition Ω_h of Ω into simple polygons P we first define the *space without boundary conditions*:

$$W_h = \{v \in H^2(\Omega) \ : \ v_{|\mathsf{P}} \in V_{h|\mathsf{P}} \ \forall \mathsf{P} \in \Omega_h\}. \tag{3.5}$$

In agreement with the *local choice* of the degrees of freedom of the previous subsection, in W_h we choose the following *global* degrees of freedom:

- $\mathcal{V}^h$: the value of v_h and ∇v_h at the vertices of $\mathcal{V}$;
- $\mathcal{E}^h$: the value of v_h and of $\partial v_h/\partial n$ at, respectively, the $\mathcal{N}_0^m$ and $\mathcal{N}_1^m$ internal nodes defined in subsection 3.2 for each edge e of $\mathcal{E}$;
- $\mathcal{P}^h$: the value of the moments

  $$\frac{1}{|\mathsf{P}|} \int_{\mathsf{P}} q(\mathbf{x}) v_h(\mathbf{x})\, dV \qquad \forall q \in \mathcal{M}_{m-2}(\mathsf{P})$$

  in each polygonal cell P.

Finally, the discrete space $V_h = W_h \cap H^1_0(\Omega)$ is given by

$$V_h = \Big\{ v \in H^2(\Omega) \ : \ v_{|\mathsf{P}} \in V_{h|\mathsf{P}} \ \forall \mathsf{P} \in \Omega_h, \ v_{|\partial\Omega} = 0 \Big\}. \tag{3.6}$$

Note that the condition $v_h \in V_h$ implies $v_h = 0$ on the vertices and the edges of the boundary $\partial\Omega$. Therefore, the degrees of freedom of V_h are simply the ones introduced above, excluding the nodal degrees of freedom associated with the function values (but not the derivatives) of the boundary vertices and edges.

3.4. Construction of $\mathcal{A}_h$. We build the discrete bilinear form $\mathcal{A}_h$ by assembling the local bilinear forms $\mathcal{A}_{h,\mathsf{P}}$ in accordance with

$$\mathcal{A}_h\big(w_h, v_h\big) = \sum_{\mathsf{P} \in \Omega_h} \mathcal{A}_{h,\mathsf{P}}\big(w_h, v_h\big) \qquad \forall w_h, v_h \in V_h. \tag{3.7}$$

The local bilinear forms $\mathcal{A}_{h,\mathsf{P}}$ are all *symmetric* and satisfy the following fundamental properties of *consistency* and *stability*.

- **Consistency:** for all h and for all P in Ω_h it holds

$$\mathcal{A}_{h,\mathsf{P}}\big(p, v_h\big) = \mathcal{A}_{\mathsf{P}}\big(p, v_h\big) \qquad \forall p \in \mathbb{P}_m(\mathsf{P}), \ \forall v_h \in V_{h|\mathsf{P}}. \tag{3.8}$$

- **Stability**: there exist two positive constants α_* and α^*, independent of h and P, such that

$$\alpha_* \, \mathcal{A}_{\mathsf{P}}\big(v_h, v_h\big) \le \mathcal{A}_{h,\mathsf{P}}\big(v_h, v_h\big) \le \alpha^* \, \mathcal{A}_{\mathsf{P}}\big(v_h, v_h\big) \qquad \forall v_h \in V_{h|\mathsf{P}}. \tag{3.9}$$

Let us assume that condition (3.8) is true and integrate by parts:

$$\begin{aligned} \mathcal{A}_{h,\mathsf{P}}\big(p, v_h\big) &= \int_\Omega \nabla p \cdot \nabla v_h \, dV \\ &= -\int_{\mathsf{P}} \Delta p \, v_h \, dV + \int_{\partial\mathsf{P}} (\mathbf{n}_{\mathsf{P}} \cdot \nabla p) \, v_h \, dS. \end{aligned} \tag{3.10}$$

Since $\Delta p \in \mathbb{P}_{m-2}(\mathsf{P})$, the first integral in the right-hand side of (3.10) can be expressed through the polynomial moments of v_h, and can, thus, be computed exactly by using its internal degrees of freedom. On the other hand, it holds that $(\mathbf{n}_{\mathsf{P}} \cdot \nabla p) \in \mathbb{P}_{m-1}(\mathsf{e})$ and $v_{h|\mathsf{e}} \in \mathbb{P}_{\alpha_0}(\mathsf{e})$ for all $\mathsf{e} \subset \partial\mathsf{P}$, so that the second integral in the right-hand side of (3.10) can be computed exactly. Therefore, the right hand side of (3.8) can be computed explicitly without knowing v_h in the interior of P. We formally summarize this result for future reference in the paper in the following remark.

REMARK 3.4. *The local degrees of freedom allow us to compute exactly $\mathcal{A}_{h,\mathsf{P}}\big(p, v_h\big)$ for any $p \in \mathbb{P}_m(\mathsf{P})$ and for any $v_h \in V_{h|\mathsf{P}}$.*

We are left to show how to construct a computable $\mathcal{A}_h$ that satisfies (3.8) and (3.9). We review such construction in section 3.6 and we refer the reader interested to alternative possibilities to [4, 9].

3.5. Construction of the loading term. Let us define the function f_h on each element P of Ω_h as the $L^2(\mathsf{P})$-projection of the function f onto the space $\mathbb{P}_{m-2}$, that is,

$$f_h = \pi^{\mathsf{P}}_{m-2}(f) \qquad \text{on each } \mathsf{P} \in \Omega_h.$$

The loading term can be written as

$$\begin{aligned}\big(f_h, v_h\big) &= \sum_{\mathsf{P}\in\Omega_h} \int_{\mathsf{P}} f_h\, v_h\, dV = \sum_{\mathsf{P}\in\Omega_h} \int_{\mathsf{P}} \pi^{\mathsf{P}}_{m-2}(f)\, v_h\, dV \\ &= \sum_{\mathsf{P}\in\Omega_h} \int_{\mathsf{P}} \pi^{\mathsf{P}}_{m-2}(f)\, \pi^{\mathsf{P}}_{m-2}(v_h)\, dV = \sum_{\mathsf{P}\in\Omega_h} \int_{\mathsf{P}} f\, \pi^{\mathsf{P}}_{m-2}(v_h)\, dV\end{aligned}$$

where the last two identities follows from the fact that $\pi^{\mathsf{P}}_{m-2}(v_h)$ is the L^2 orthogonal projection of f onto $\mathbb{P}_{m-2}(\mathsf{P})$, and that v_h and $\pi^{\mathsf{P}}_{m-2}(v_h)$ have the same internal moments. Thus, the right-hand side of (3.1) can be computed exactly by using the degrees of freedom of the functions in V_h that represent the internal moments.

3.6. Implementation of the local stiffness matrices. In this section, we review the mimetic construction of the local stiffness matrix M_P, which is associated with the local bilinear form $\mathcal{A}_{h,\mathsf{P}}$.

For each polygonal cell $\mathsf{P} \in \Omega_h$, the elemental stiffness matrix M_P is such that

$$\mathcal{A}_{h,\mathsf{P}}\big(w_{h,\mathsf{P}}, v_{h,\mathsf{P}}\big) = \underline{w}^T_{h,\mathsf{P}}\, \mathsf{M}_\mathsf{P}\, \underline{v}_{h,\mathsf{P}} \qquad \forall w_{h,\mathsf{P}},\ v_{h,\mathsf{P}} \in \mathcal{V}^h_\mathsf{P},$$

where the vectors $\underline{w}_{h,\mathsf{P}}$ and $\underline{v}_{h,\mathsf{P}}$ represents the values of the local degrees of freedom of $w_{h,\mathsf{P}}$ and $v_{h,\mathsf{P}}$. The global stiffness matrix is then obtained by a standard finite element-like assembly procedure.

For the mimetic construction of M_P, we need two matrices N_P and R_P that satisfy an algebraic form of the consistency condition (S1), i.e., that are such that $\mathsf{M}_\mathsf{P}\mathsf{N}_\mathsf{P} = \mathsf{R}_\mathsf{P}$ and such that $\mathsf{N}^T_\mathsf{P}\mathsf{R}_\mathsf{P}$ is a symmetric and nonnegative definite matrix. Let p_i be the i-th element of the basis $\mathcal{M}_m(\mathsf{P})$ of the polynomial space $\mathbb{P}_m(\mathsf{P})$. The index i runs from 1 to $\mathcal{N}^m = (m+1)(m+2)/2$, the cardinality of $\mathcal{M}_m(\mathsf{P})$, and suitably renumbers the monomials forming such basis, e.g.,

$$p_1(x,y) = 1, \quad p_2(x,y) = (x - x_\mathsf{P})/h_\mathsf{P}, \quad p_3(x,y) = (y - y_\mathsf{P})/h_\mathsf{P}, \quad \text{etc.}$$

Let $\mathcal{N}^m_\mathsf{P}$ denote the dimension of $V_{h|\mathsf{P}}$ and χ_i for $i = 1, \ldots, \mathcal{N}^m_\mathsf{P}$ the operator returning the i-th local degree of freedom. The j-th column of matrix $\mathsf{N}_\mathsf{P} \in \mathbb{R}^{\mathcal{N}^m_\mathsf{P} \times \mathcal{N}^m}$ is formed by the degrees of freedom of the j-th polynomial p_j of $\mathcal{M}_m(\mathsf{P})$; thus, the (ij)-th entry of N_P is given by

$$\big(\mathsf{N}_\mathsf{P}\big)_{ij} = \chi_i(p_j) \qquad \text{for } i = 1, \ldots, \mathcal{N}^m_\mathsf{P},\ j = 1, \ldots, \mathcal{N}^m. \tag{3.11}$$

The j-th column of matrix $\mathsf{R}_\mathsf{P} \in \mathbb{R}^{\mathcal{N}^m_\mathsf{P} \times \mathcal{N}^m}$ is given by the right-hand side of the consistency condition (3.8) applied to the j-th polynomial p_j of $\mathcal{M}_m(\mathsf{P})$. To write an expression for such matrix we introduce the unique function $\varepsilon^i_{h,\mathsf{P}}$ of $\mathcal{V}^h_\mathsf{P}$ that is such that $\chi_j(\varepsilon^i_{h,\mathsf{P}}) = \delta_{ij}$ for $i, j = 1, \ldots, \mathcal{N}^m_\mathsf{P}$. Using such function, the (ij)-th entry of matrix R_P takes the form:

$$\big(\mathsf{R}_\mathsf{P}\big)_{ij} = \int_\Omega \nabla p_j \cdot \nabla \varepsilon^i_{h,\mathsf{P}}\, dV \qquad \text{for } i = 1, \ldots, \mathcal{N}^m_\mathsf{P},\ j = 1, \ldots, \mathcal{N}^m. \tag{3.12}$$

In view of Remark 3.4 (see, also, the development in (3.10)) the right-hand side of (3.12) is computable exactly.

From the definitions above it is easy to show that $\mathsf{M}_\mathsf{P}\mathsf{N}_\mathsf{P} = \mathsf{R}_\mathsf{P}$, which is the matrix form of the consistency condition (3.8). Furthermore, a straightforward calculation shows that

$$\left(\mathsf{N}_\mathsf{P}^T\mathsf{R}_\mathsf{P}\right)_{ij} = \int_\mathsf{P} \nabla p_i \cdot \nabla p_j \, dV, \tag{3.13}$$

so that $\mathsf{N}_\mathsf{P}^T\mathsf{R}_\mathsf{P}$ is symmetric and semi-positive definite. Let K_P be the square symmetric matrix that represents the bilinear form $\mathcal{A}_h$ restricted to the space $\mathbb{P}_m(\mathsf{P})$. Clearly, it holds that

$$\mathsf{K}_\mathsf{P} = \mathsf{N}_\mathsf{P}^T\mathsf{M}_\mathsf{P}\mathsf{N}_\mathsf{P} = \mathsf{N}_\mathsf{P}^T\mathsf{R}_\mathsf{P}, \tag{3.14}$$

where matrix $\mathsf{K}_\mathsf{P} \in \mathbb{R}^{\mathcal{N}^m \times \mathcal{N}^m}$ has the block-diagonal form

$$\mathsf{K}_\mathsf{P} = \begin{pmatrix} 0 & \mathbf{0} \\ \mathbf{0} & \widehat{\mathsf{K}}_\mathsf{P} \end{pmatrix}$$

and $\widehat{\mathsf{K}}_\mathsf{P} \in \mathbb{R}^{(\mathcal{N}^m-1)\times(\mathcal{N}^m-1)}$ is a strictly positive definite matrix. Let $\mathsf{K}_\mathsf{P}^\dagger \in \mathbb{R}^{\mathcal{N}^m \times \mathcal{N}^m}$ be the pseudo-inverse of matrix K_P, which we define as

$$\mathsf{K}_\mathsf{P}^\dagger = \begin{pmatrix} 0 & \mathbf{0} \\ \mathbf{0} & \widehat{\mathsf{K}}_\mathsf{P}^{-1} \end{pmatrix}.$$

Eventually, we define the local stiffness matrix

$$\mathsf{M}_\mathsf{P} = \mathsf{R}_\mathsf{P}\mathsf{K}_\mathsf{P}^\dagger\mathsf{R}_\mathsf{P}^T + \eta_\mathsf{P}\,\mathsf{P}_\mathsf{P}, \tag{3.15}$$

where the positive real number η_P is equal to the trace of $\mathsf{R}_\mathsf{P}\mathsf{K}_\mathsf{P}^\dagger\mathsf{R}_\mathsf{P}^T$, and

$$\mathsf{P}_\mathsf{P} = \mathsf{I} - \mathsf{N}_\mathsf{P}\left(\mathsf{N}_\mathsf{P}^T\mathsf{N}_\mathsf{P}\right)^{-1}\mathsf{N}_\mathsf{P}^T,$$

where I is the (properly sized) identity matrix. Note that matrix P_P is the projector to the orthogonal complement of the space spanned by the columns of matrix N_P and that the product $\mathsf{P}_\mathsf{P}\mathsf{N}_\mathsf{P}$ is zero. Therefore, also due to (3.14), we immediately have the consistency condition (3.8) in the matrix form $\mathsf{M}_\mathsf{P}\mathsf{N}_\mathsf{P} = \mathsf{R}_\mathsf{P}$. The purpose of the second matrix in (3.15) is to guarantee the stability condition expressed by (3.9), and, thus, the coercivity (up to the correct kernel) of the system.

3.7. A priori error estimates. Let us introduce the following mesh assumptions.

ASSUMPTION 3.2 (Mesh regularity). *There exists a real number $\gamma > 0$ such that, for all h, each element P in Ω_h is star-shaped with respect to a ball of radius $\geq \gamma h_\mathsf{P}$, where h_P is the diameter of P. Moreover, there exists a real number $\gamma' > 0$ such that, for all h and for each element P in Ω_h, the distance between any two vertices of P is $\geq \gamma' h_\mathsf{P}$.*

Then, the following convergence theorem holds, see [9] for the proof.

THEOREM 3.3. *Let the consistency and stability conditions* (3.8)-(3.9) *and the mesh assumptions considered above hold. Then, the discrete problem* (3.1) *has a unique solution and, if the solution u of* (2.3) *belongs to $H^2(\Omega)$, it holds that*

$$|u - u_h|_1 \leq Ch^s \, |u|_{s+1} \tag{3.16}$$

for all $2 \leq s \leq m$, where C is a constant independent of h.

The condition $u \in H^2(\Omega)$ can be locally relaxed. In fact, the method considered herein can be easily adapted in order to make use of a less regular space V_h across *selected vertices and edges* of the mesh, see [9].

4. A reliable error estimator. In this section we present the error estimator and prove its reliability. Through the rest of the paper we will assume the mesh conditions introduced in Section 3.7.

4.1. The error estimator. In order to introduce the error estimator we need a pair of preliminary definitions.

We start introducing, for all $\mathsf{P} \in \Omega_h$, the following energy projection $\Pi^{\mathsf{P}}_m : H^1(\mathsf{P}) \to \mathbb{P}_{m,0}(\mathsf{P})$, where $\mathbb{P}_{m,0}$ indicates the subpace of $\mathbb{P}_m$ of polynomials with zero average. For all $v \in H^1(\mathsf{P})$, the image $\Pi^{\mathsf{P}}_m v \in \mathbb{P}_{m,0}(\mathsf{P})$ is uniquely defined as the energy projection

$$\mathcal{A}_{\mathsf{P}}\big(\Pi^{\mathsf{P}}_m v, p\big) = \mathcal{A}_{\mathsf{P}}\big(v, p\big) \qquad \forall p \in \mathbb{P}_{m,0}(\mathsf{P}). \tag{4.1}$$

Note that, due to the consistency condition, if $v_h \in V_{h|\mathsf{P}} \subset H^1(\mathsf{P})$, then (4.1) is equivalent to

$$\mathcal{A}_{h,\mathsf{P}}\big(\Pi^{\mathsf{P}}_m v_h, p\big) = \mathcal{A}_{h,\mathsf{P}}\big(v_h, p\big) \qquad \forall p \in \mathbb{P}_{m,0}(\mathsf{P}). \tag{4.2}$$

Therefore $\Pi^{\mathsf{P}}_m v_h$ is explicitly computable for any function $v_h \in V_{h|\mathsf{P}}$.

We now recall that π^{P}_m represents the $L^2(\mathsf{P})$ projection on $\mathbb{P}_m(\mathsf{P})$. For all $v_{h,\mathsf{P}} \in V_{h|\mathsf{P}}$ and $\mathsf{P} \in \Omega_h$ the projection $\pi^{\mathsf{P}}_m(\Delta v_h)$ is explicitly computable. Indeed, integrating twice by parts, for all $p \in \mathbb{P}_m(\mathsf{P})$ it holds

$$\int_{\mathsf{P}} (\Delta v_{h,\mathsf{P}}) p \, dV = \int_{\mathsf{P}} v_{h,\mathsf{P}} (\Delta p) \, dV + \int_{\partial\mathsf{P}} p (\nabla v_{h,\mathsf{P}}) \cdot \mathbf{n}_{\mathsf{P}} \, dS - \int_{\partial\mathsf{P}} v_{h,\mathsf{P}} (\nabla p) \cdot \mathbf{n}_{\mathsf{P}} \, dS$$

The first term in the right hand side is computable using the internal degrees of freedom since $(\Delta p) \in \mathbb{P}_{m-2}(\mathsf{P})$, while the remainig terms are boundary terms involving v_h and its normal derivative, that are known explicitly.

We can now introduce, for all $\mathsf{P} \in \Omega_h$, the following *local* and *computable* terms:

$$\begin{aligned} \eta^r_{\mathsf{P}} &= h_{\mathsf{P}} || f + \pi^{\mathsf{P}}_m(\Delta u_{h,\mathsf{P}}) ||_{L^2(\mathsf{P})}, \\ \eta^l_{\mathsf{P}} &= h_{\mathsf{P}} || f - f_h ||_{L^2(\mathsf{P})}, \\ \eta^c_{\mathsf{P}} &= \mathcal{A}_{h,\mathsf{P}}\big(u_{h,\mathsf{P}} - \Pi^{\mathsf{P}}_m u_{h,\mathsf{P}}, u_{h,\mathsf{P}} - \Pi^{\mathsf{P}}_m u_{h,\mathsf{P}}\big)^{1/2}, \end{aligned} \tag{4.3}$$

where u_h is the solution of the discrete problem and $u_{h,\mathsf{P}}$ its restriction to the generic element P.

The first term, where a kind of discrete residual appears, represents an estimation of the error stemming from the Galerkin discretization of the problem. The second term estimates the right hand side approximation. The third term bounds the error related to the inconsistency between the continuous and discrete bilinear forms, $\mathcal{A}(\cdot,\cdot)$ and $\mathcal{A}_h(\cdot,\cdot)$.

The result here below shows the reliability of the proposed error estimator η; the proof is postponed in the following section.

THEOREM 4.1. *Let u_h be the solution of* (3.1) *and u the solution of* (2.3). *Let the global error estimator*

$$\eta^2 = \sum_{\mathsf{P} \in \Omega_h} \eta^2_{\mathsf{P}}, \qquad \textit{where} \qquad \eta^2_{\mathsf{P}} = (\eta^r_{\mathsf{P}})^2 + (\eta^l_{\mathsf{P}})^2 + (\eta^c_{\mathsf{P}})^2 \quad \forall \mathsf{P} \in \Omega_h.$$

Then, under the mesh assumptions above, it exists a constant C independent of h such that

$$||u - u_h||_{H^1(\mathsf{P})} \leq C\eta.$$

Since the above estimator η^2 is the sum of local terms, it can be used for an adaptive mesh generation strategy, as will be shown in the numerical tests section. Note that, differently from standard FEM residual estimators, there are no jump terms since the solution u_h is globally C^1.

We continue this section with some observations regarding the consistency estimator η^c_{P}, since this is the less standard term among the ones above. First of all we note that η^c_{P} can be computed in a very direct way, if one follows the stiffness matrix construction given in Section 3.6. Indeed, writing (4.2) and $(4.3)_3$ in terms of matrixes, using definition (3.15) and property (3.14), after some algebra one gets

$$(\eta^c_{\mathsf{P}})^2 = \eta \ \underline{u}^T_{h,\mathsf{P}} \ \mathsf{P}_{\mathsf{P}} \ \underline{u}_{h,\mathsf{P}}$$

where as usual the vector $\underline{u}_{h,\mathsf{P}}$ represents the local degree of freedom of values of $u_{h,\mathsf{P}}$.

Regarding the asymptotic behavior of such term, we can observe the following. Since the bilinear form $\mathcal{A}_{\mathsf{P}}(\cdot,\cdot)$ is, up to uniform constants, equivalent to the H^1 squared seminorm, it is immediate to check that the energy projector Π^{P}_m is continuous from $H^1(\mathsf{P})$ to $H^1(\mathsf{P})$. Therefore, property (3.9), triangle inequalities and the continuity of Π^{P}_m yield

$$\begin{aligned}(\eta^c_{\mathsf{P}})^2 &= \mathcal{A}_{h,\mathsf{P}}\big(u_{h,\mathsf{P}} - \Pi^{\mathsf{P}}_m u_{h,\mathsf{P}}, u_{h,\mathsf{P}} - \Pi^{\mathsf{P}}_m u_{h,\mathsf{P}}\big) \le C|u_h - \Pi^{\mathsf{P}}_m u_h|^2_{H^1(\mathsf{P})} \\ &\le C\big(|u-u_h|^2_{H^1(\mathsf{P})} + |u - \Pi^{\mathsf{P}}_m u|^2_{H^1(\mathsf{P})} + |\Pi^{\mathsf{P}}_m(u-u_h)|^2_{H^1(\mathsf{P})}\big) \\ &\le C\big(|u-u_h|^2_{H^1(\mathsf{P})} + |u - \Pi^{\mathsf{P}}_m u|^2_{H^1(\mathsf{P})}\big).\end{aligned}$$

The first term in the right hand side above is the local error, while the second term is an approximation term that, by standard polynomial approximation estimates, can be bounded by

$$|u - \Pi^{\mathsf{P}}_m u|^2_{H^1(\mathsf{P})} \le C\, h^{2s}_{\mathsf{P}}\, |u|^2_{H^{s+1}(\mathsf{P})}$$

for all $0 \le s \le m$, provided $u_{|\mathsf{P}}$ is sufficiently regular. Therefore the asymptotic behavior of η^c_{P} is expected to be the same as the error.

As a consequence of Theorem 4.1, the consistency term η^c_{P} should be kept into the estimator as a safeguard (so that reliability is guaranteed) but possibly should not dominate the other terms. In other words we expect that, in practice, it may give slightly better adaptive results to consider an estimator in which term is scaled by a small constant.

4.2. Proof of Theorem 4.1. In this section we show the proof of Theorem 4.1. We will make use of the following two lemmas. Note that in general we cannot apply standard scaling arguments since the functions of $V_{h|\mathsf{P}}$ are not associated to a fixed reference space (independent of P) on some reference element.

LEMMA 4.2. *It exists a constant C independent of h such that*

$$h_{\mathsf{P}}|v_h|_{H^2(\mathsf{P})} \ \le \ C\,|v_h|_{H^1(\mathsf{P})} \qquad \forall \mathsf{P} \in \Omega_h, \ \forall v_h \in V_{h|\mathsf{P}}. \tag{4.4}$$

Proof. We start observing that, due to the mesh assumptions above, it is easy to check that all the elements in $\{\Omega_h\}_h$ are polygons with at most N edges, with N independent of h. Therefore it is not restrictive to assume that the number of

edges $3 \leq n \leq N$ is fixed. Given any polygon P of the mesh family with n edges, let $X = \{X_1, X_2, ..., X_n\}$ represent the position of the n (anti-clockwise) vertexes defining $\mathsf{P} = \mathsf{P}(X)$. Since equation (4.4) scales with the size of the element, it is not restrictive to assume that the diameter $h_{\mathsf{P}} = 1$ and, by a simple translation, that $X_1 = (0, 0)$. Since the space $V_{h|\mathsf{P}}$ is finite dimensional, it clearly holds

$$h_{\mathsf{P}}|v_h|_{H^2(\mathsf{P})} \leq C\,|v_h|_{H^1(\mathsf{P})} \qquad \forall v_h \in V_{h|\mathsf{P}}, \tag{4.5}$$

with the constant C=C(X) depending on X.

Due to the diameter property above, the set Σ of vectors $X \in \mathbb{R}^{2n}$ representing all possible polygons P with n edges constitutes a bounded set. Moreover it can be checked that, due to the mesh regularity assumptions and property $h_{\mathsf{P}} = 1$, such set is also closed. In fact, such regularity property forbids the vectors in Σ to be arbitrarily close to inadmissible vectors $\bar{X} \notin \Sigma$, like those where two vertexes are collapsed into a single vertex. Thus Σ forms a compact set. Therefore, indicating with C the (4.5) constant associated to the element P defined by X, all we need to show is that the function

$$C(X) = \sup_{v_h \in V_{h|\mathsf{P}}/\mathbb{R}} \frac{h_{\mathsf{P}}|v_h|_{H^2(\mathsf{P})}}{|v_h|_{H^1(\mathsf{P})}}$$

is a continuous function of X. The maximum of such function on Σ will then yield the constant appearing in (4.4).

Let now $\{X_k\}$ be a sequence converging to X, and let P_k be the polygon associated to X_k, $k \in \mathbb{N}$. Let v_h be any function in $V_{h|\mathsf{P}}$. Then, for all k, we can build a function in $v_h^k \in V_{h|\mathsf{P}_k}$ by selecting the same degrees of freedom values (with corresponding vertexes and edges) as those of v_h on the element P_k. Moreover, for k sufficiently large, it can always be built a sequence ϕ^k of $W^{2,\infty}$ invertible mappings from P to P_k, such that ϕ^k converge the the identity (in $W^{2,\infty}$) as $k \to \infty$. Using such mappings it can then be shown that, as $X_k \to X$, the seminorms $|v_h^k|_{H^s(\mathsf{P}_k)} \to |v_h|_{H^s(\mathsf{P})}$, $s = 1, 2$. This can be done by checking that $v_h^k \circ \phi^k$ converges to v_h in $H^2(\mathsf{P})$. Without showing the details, such calculation involves writing the biharmonic variational problem associated to the definition of $V_{h|\mathsf{P}}$ and $V_{h|\mathsf{P}_k}$, a change of variables through the mapping ϕ^k, and noting that the ϕ^k converge to the identity in $W^{2,\infty}$ as $X^k \to X$. The construction above immediately implies that

$$\lim_{k\to\infty} C(X_k) \geq C(X).$$

The converse is shown with an analogous reasoning in the opposite direction. □

With an analogous argument also the following inverse estimate, useful in the proof of the next Lemma, can be shown:

$$h_{\mathsf{P}}|v_h|_{H^1(\mathsf{P})} \leq C\,||v_h||_{L^2(\mathsf{P})} \qquad \forall \mathsf{P} \in \Omega_h,\ \forall v_h \in V_{h|\mathsf{P}}. \tag{4.6}$$

LEMMA 4.3. *It exists a Clément-type interpolant $H_0^1(\Omega) \to V_h$ such that for any function $v \in H_0^1(\Omega)$ and all $\mathsf{P} \in \Omega_h$, the interpolant $v_{\mathfrak{C}}$ satisfies*

$$||v - v_{\mathfrak{C}}||_{L^2(\mathsf{P})} + h_{\mathsf{P}}|v_{\mathfrak{C}}|_{H^1(\mathsf{P})} \leq Ch_{\mathsf{P}}|v|_{H^1(\omega_{\mathsf{P}})} \tag{4.7}$$

with C independent of h and where ω_{P} is the union of all elements P that share a vertex with P.

Proof. Let the subspace $\widehat{V}_h \subset V_h$ be defined as the space of all functions in V_h such that all degrees of freedom values associated to pointwise derivatives and first or higher order moments are null. Let now Ξ_h indicate the set of all vertexes and edge nodes of Ω_h associated to degrees of freedom that are pointwise evaluations, i.e. the set of all nodes associated to $\mathcal{V}^h$ and $\mathcal{E}^h$ for derivative order $j = 0$. Then, given any $v \in H_0^1\Omega$, we define $v_{\mathfrak{C}} \subset \widehat{V}_h$ by

$$\begin{cases} v_{\mathfrak{C}}(\nu) = \dfrac{1}{|\omega_\nu|}\displaystyle\int_\nu v\, dV \qquad \forall \nu \in \Xi_h, \\ \dfrac{1}{|\mathsf{P}|}\displaystyle\int_{\mathsf{P}} v_{\mathfrak{C}}\, dV = \dfrac{1}{N^{\mathcal{E}}_{\mathsf{P}}}\displaystyle\sum_{\mathsf{v}\in\partial\mathsf{P}} v(\mathsf{P}) \qquad \mathsf{P} \in \Omega_h, \end{cases} \tag{4.8}$$

where as usual the symbol v indicates a generic vertex and

$$\omega_\nu = \{\cup\, \mathsf{P} \,:\, \nu \in \partial\mathsf{P}\}.$$

Note that, for all $\mathsf{P} \in \Omega_h$, if $v : \omega_{\mathsf{P}} \to \mathbb{R}$ is constant, then $v_{\mathfrak{C}}|_{\mathsf{P}} = v|_{\mathsf{P}}$; the above operator preserves local constants. Assume that the following continuity property holds

$$||v_{\mathfrak{C}}||_{L^2(\mathsf{P})} \le C||v||_{L^2(\omega_{\mathsf{P}})} \qquad \forall \mathsf{P} \in \Omega_h,\ \forall v \in H_0^1(\Omega). \tag{4.9}$$

with C independent of h and $\mathsf{P} \in \Omega_h$.

Then, for all $v \in H_0^1(\Omega)$ and $\mathsf{P} \in \Omega_h$, let $\overline{v}$ denote the average of v on ω_{P}. First by a triangle inequality and recalling that the operator preserves constants, then using (4.9), finally by standard approximation estimates on star shaped domains, we get

$$\begin{aligned} ||v - v_{\mathfrak{C}}||_{L^2(\mathsf{P})} &\le ||v - \overline{v}||_{L^2(\mathsf{P})} + ||(v-\overline{v})_{\mathfrak{C}}||_{L^2(\mathsf{P})} \\ &\le C||v - \overline{v}||_{L^2(\omega_{\mathsf{P}})} \le Ch_{\mathsf{P}}|v|_{H^1(\omega_{\mathsf{P}})} \end{aligned}$$

that is a part of (4.7).

The remaining part follows by using again the constant preserving property, inverse estimate (4.6), bound (4.9) and standard approximation properties

$$\begin{aligned} |v_{\mathfrak{C}}|^2_{H^1(\mathsf{P})} = |(v-\overline{v})_{\mathfrak{C}}|^2_{H^1(\mathsf{P})} &\le C(h_{\mathsf{P}})^{-2}||(v-\overline{v})_{\mathfrak{C}}||^2_{L^2(\mathsf{P})} \\ &\le C(h_{\mathsf{P}})^{-2}||v-\overline{v}||^2_{L^2(\omega_{\mathsf{P}})} \le C|v|_{H^1(\omega_{\mathsf{P}})}. \end{aligned}$$

Therefore we are left to show (4.9). By definition of $v_{\mathfrak{C}}$, it can be easily checked that

$$\sum_{\nu\in\Xi_h\cap\partial\mathsf{P}} |v_{\mathfrak{C}}(\nu)|^2 + \Big|\frac{1}{|\mathsf{P}|}\int_{\mathsf{P}} v_{\mathfrak{C}}\, dV\Big|^2 \le C||v||^2_{L^2(\omega_{\mathsf{P}})}$$

for all $\mathsf{P} \in \Omega_h, v \in H_0^1(\Omega)$. Bound (4.9) is therefore proved if we show the existence of a uniform constant C such that

$$||v_h||^2_{L^2(\Omega)} \le C\Big(\sum_{\nu\in\Xi_h\cap\partial\mathsf{P}} |v_h(\nu)|^2 + \Big|\frac{1}{|\mathsf{P}|}\int_{\mathsf{P}} v_h\, dV\Big|^2\Big) \qquad \forall v_h \in \widehat{V}_h. \tag{4.10}$$

The latter bound is not shown here, as it can be proved with the same technique as in the proof of Lemma 4.3. One has essentially to show that, once the values of

degrees of freedom of $v_h \in \widehat{V}_h$ are fixed, both left and right hand sides in (4.10) vary continuously with respect to $\mathsf{P} = \mathsf{P}(X)$ for $X \in \Sigma$. □

We can now show the proof of Theorem 4.1. Let the error $e = u - u_h$. First using the stability property (3.9) and the coercivity of $\mathcal{A}\big(\cdot,\cdot\big)$, then by simple manipulations, we obtain

$$\widetilde{\alpha}\,|u-u_h|^2_{H^1\Omega} \le \mathcal{A}\big(u-u_h, e\big) = T_r + T_l + T_c, \tag{4.11}$$

where $\widetilde{\alpha}$ is a strictly positive constant and

$$\begin{aligned} T_r &= \mathcal{A}\big(u-u_h, e-e_{\mathfrak{C}}\big),\\ T_l &= \mathcal{A}\big(u, e_{\mathfrak{C}}\big) - \mathcal{A}_h\big(u_h, e_{\mathfrak{C}}\big),\\ T_c &= \mathcal{A}_h\big(u_h, e_{\mathfrak{C}}\big) - \mathcal{A}\big(u_h, e_{\mathfrak{C}}\big). \end{aligned}$$

We first bound the term T_r. We apply equation (2.3), integrate by parts on the *whole* domain Ω recalling that $u_h \in H^2(\Omega)$, use the Cauchy-Schwarz inequality and Lemma 4.3 to obtain

$$\begin{aligned} T_r = (f, e-e_{\mathfrak{C}}) + (\Delta u_h, e-e_{\mathfrak{C}}) &\le \sum_{\mathsf{P}\in\Omega_h} ||f+\Delta u_h||_{L^2(\mathsf{P})}||e-e_{\mathfrak{C}}||_{L^2(\mathsf{P})}\\ &\le \sum_{\mathsf{P}\in\Omega_h} h_{\mathsf{P}}||f+\Delta u_h||_{L^2(\mathsf{P})}|e|_{H^1(\omega_{\mathsf{P}})} \le C\Big(\sum_{\mathsf{P}\in\Omega_h} h^2_{\mathsf{P}}||f+\Delta u_h||^2_{L^2(\mathsf{P})}\Big)^{1/2}|e|_{H^1(\Omega)}. \end{aligned} \tag{4.12}$$

By definition of L^2 projection and since $\Delta\Pi^{\mathsf{P}}_m u_h \in \mathbb{P}_0(\mathsf{P}) \subset \mathbb{P}_m(\mathsf{P})$, it holds

$$h_{\mathsf{P}}||\Delta u_h - \pi^{\mathsf{P}}_m \Delta u_h||_{L^2(\mathsf{P})} \le h_{\mathsf{P}}||\Delta u_h - \Delta\Pi^{\mathsf{P}}_m u_h||_{L^2(\mathsf{P})}. \tag{4.13}$$

The inverse estimate in Lemma 4.2, the coercivity of $\mathcal{A}_{\mathsf{P}}\big(\cdot,\cdot\big)$ and the stability property (3.9) yield from (4.13)

$$\begin{aligned} h_{\mathsf{P}}||\Delta u_h - \pi^{\mathsf{P}}_m \Delta u_h||_{L^2(\mathsf{P})} &\le h_{\mathsf{P}}|u_h - \Pi^{\mathsf{P}}_m u_h|_{H^2(\mathsf{P})} \le C|u_h - \Pi^{\mathsf{P}}_m u_h|_{H^1(\mathsf{P})}\\ &\le C\mathcal{A}_{\mathsf{P}}\big(u_h - \Pi^{\mathsf{P}}_m u_h, u_h - \Pi^{\mathsf{P}}_m u_h\big)^{1/2} \le C\,\eta^c_{\mathsf{P}}. \end{aligned} \tag{4.14}$$

Combining (4.12) with (4.14) it easily follows

$$T_r \le C\Big(\sum_{\mathsf{P}\in\Omega_h} h^2_{\mathsf{P}}||f+\Delta u_h||^2_{L^2(\mathsf{P})} + (\eta^c_{\mathsf{P}})^2\Big)^{1/2}|e|_{H^1(\Omega)}. \tag{4.15}$$

In order to bound T_l, we start observing that, by (2.3) and (3.1) ,

$$T_l = (f, e_{\mathfrak{C}}) - (f_h, e_{\mathfrak{C}})$$

Let now $\overline{e}_{\mathfrak{C}}$ be the piecewise constant function given, on each element P, by the average of $e_{\mathfrak{C}}$ on P. Then, since on each element $f_h = \pi^{\mathsf{P}}_{m-2}(f)$ and $m \ge 2$, it holds

$$T_l = (f-f_h, e_{\mathfrak{C}} - \overline{e}_{\mathfrak{C}}) \le \sum_{\mathsf{P}\in\Omega_h} ||f-f_h||_{L^2(\mathsf{P})}||e_{\mathfrak{C}} - \overline{e}_{\mathfrak{C}}||_{L^2(\mathsf{P})}. \tag{4.16}$$

Applying standard error estimates and recalling Lemma 4.3 yields from (4.16)

$$T_l \le C\sum_{\mathsf{P}\in\Omega_h} \eta^l_{\mathsf{P}}\,|e_{\mathfrak{C}}|_{H^1(\mathsf{P})} \le C\Big(\sum_{\mathsf{P}\in\Omega_h} (\eta^l_{\mathsf{P}})^2\Big)^{1/2}|e|_{H^1(\Omega)}. \tag{4.17}$$

We now bound the last term. Using the consistency property (3.8), then the Cauchy-Schwarz inequality on both bilinear forms gives

$$\begin{aligned} T_c &= \mathcal{A}_h\big(u_h, e_{\mathfrak{C}}\big) - \mathcal{A}\big(u_h, e_{\mathfrak{C}}\big) = \mathcal{A}_h\big(u_h - \Pi_m^{\mathsf{P}} u_h, e_{\mathfrak{C}}\big) - \mathcal{A}\big(u_h - \Pi_m^{\mathsf{P}} u_h, e_{\mathfrak{C}}\big) \\ &\leq \mathcal{A}_h\big(u_h - \Pi_m^{\mathsf{P}} u_h, u_h - \Pi_m^{\mathsf{P}} u_h\big)^{1/2} \mathcal{A}_h\big(e_{\mathfrak{C}}, e_{\mathfrak{C}}\big)^{1/2} \\ &+ \mathcal{A}\big(u_h - \Pi_m^{\mathsf{P}} u_h, u_h - \Pi_m^{\mathsf{P}} u_h\big)^{1/2} \mathcal{A}\big(e_{\mathfrak{C}}, e_{\mathfrak{C}}\big)^{1/2}. \end{aligned} \tag{4.18}$$

First by the stability propery (3.9) and the H^1 continuity of $\mathcal{A}\big(\cdot,\cdot\big)$, then due to Lemma 4.3 it follows from (4.18)

$$\begin{aligned} T_c &\leq C\mathcal{A}_h\big(u_h - \Pi_m^{\mathsf{P}} u_h, u_h - \Pi_m^{\mathsf{P}} u_h\big)^{1/2} |e_{\mathfrak{C}}|_{H^1(\Omega)} \\ &\leq C\Big(\sum_{\mathsf{P}\in\Omega_h} (\eta_{\mathsf{P}}^c)^2\Big)^{1/2} |e|_{H^1(\Omega)}. \end{aligned} \tag{4.19}$$

The proof of Theorem 4.1 finally follows by combining equation (4.11) with bounds (4.15), (4.17), (4.19).

5. Numerical experiments. In this section, we investigate the behavior of the error estimator by solving the boundary value problem (2.3) in two benchmark cases that differ in the shape of the computational domain Ω and in the regularity of the exact solution. We show the performance of the estimator coupled with a simple mesh adaptive strategy by comparing the convergence errors obtained on a sequence of meshes that are either uniformly or adaptively refined starting from a given base mesh. These meshes are formed by different types of cells such as pattern-distorted quadrilaterals and hexagons. Other choices of cells were considered in a preliminary stage of this work in agreement with the mesh regularity constraint of Assumption 3.2 and using these meshes we obtained very similar results.

For the lowest-regular method (i.e., $\alpha = 0$ and $m \geq 1$), we also consider an *hp* refinement strategy based on comparing the actual solution with a reference solution. The reference solution is computed on a uniform refinement of the mesh used to compute the actual solution and by increasing the polynomial degree in each cell by 1. The comparison between the solution indicates where the accuracy of the actual numerical solution must be improved.

5.1. "h"-refinement based on a posteriori error estimation. The uniform refinement process is implemented by generating the refined mesh with a finer mesh size parameter. Specific details are given in the description of each test case. This strategy preserves the conformity and shape regularity of the mesh. Instead, an adaptively refined mesh is generated from a given mesh by refining each element that has been marked for refinement in accordance with the local error estimate provided by our error indicator. To refine a marked element P with m_{P} vertices and edges we subdivide it into m_{P} nested sub-elements by connecting the edge midpoints of each pair of consecutive edges of $\partial\mathsf{P}$ to the center of P. As all the cells of these meshes are convex, we take the barycenter of P as such internal point. All the sub-elements generated by this process are quadrilaterals disregarding the shape of the parent mesh element. Starting from the coarsest base mesh, the adaptively refinement strategy proceeds as follows:

(*i*) we calculate all the local element error indicators η_i, for $i = 1, \ldots, N_{\mathsf{P}}$;
(*ii*) we sort the element in accordance with their error estimate;

(*iii*) we mark for refinement all the elements P_i starting from the element showing the biggest estimated error until one of the two following conditions is satisfied:
  - at least 20% of the element has been marked;
  - the sum of the estimated errors η_i of the cells that are marked for refinement is bigger than an assigned fraction of the total estimated error;

(*iv*) we sub-divide all marked elements as described above.

This strategy preserves the shape regularity of the base mesh but leads in general to non-conforming meshes, which are still acceptable for the VEM. As the VEM can be applied to non-conforming meshes, we avoid the artificial refinement of neighboring elements as is required in *redbluegreen* strategies for triangular meshes. Note that the theoretical error estimates for the method are valid for mesh families with the uniform bound on the number of edges required by our mesh regularity assumptions. Therefore, we should, in principle, insert an automatic check in order to avoid an uncontrolled growth of the number of hanging nodes. However, in all the tests that we performed, the presence of such a check proved almost worthless as the number of edges per element seemed to stay naturally rather limited.

For each test case, we present a plot of the convergence errors for the uniform and the adaptive refinement, a plot for the three different terms forming the estimator, cf. (4.3), and a plot for the efficiency index, which is defined as the ratio between the estimated and the true approximation error. We also who a picture of the adaptively refined meshes at two intermediate refinement steps.

5.2. "hp"-refinement based on a reference solution. For the low-regular cases, i.e., $\alpha = 0$ and $m \geq 1$, we also developed an *hp*-refinement strategy, where the error estimation makes use of a reference solution. This method is adapted from the hp-adaptive strategy developed by Demkowicz and collaborators, see, e.g. [19, 20, 24, 25], and the refinement technique of Melenk and Wohlmuth [23]. Refinement decisions are taken by comparing the actual solution with a reference solution, and proceeds in two main steps.

(*i*) In the first step, we compute a local and global estimate of the numerical error by comparing the actual solution and a reference solution. The actual solution is computed on a given mesh Ω_h and each cell of the mesh has assigned its own polynomial degree, e.g., m_{P}. To compute the reference solution we first refine uniformly the actual mesh, i.e., $\Omega_{h+1/2}$, and, then, we increase by 1 the polynomial degree of each cell, e.g., $m_{\mathsf{P}} + 1$. The uniform refinement of the mesh is done by applying the same technique described in the previous section, i.e., by splitting each polygonal cell regardless of its geometrical shape, in quadrilateral sub-cells. Note that each edge of the actual mesh is split into two sub-edges in the uniformly refined mesh. Thus, we have the two numerical solutions available $u_{h,m}$ and $u_{h+1/2,m+1}$. Since $u_{h+1/2,m+1}$ is more accurate than $u_{h,m}$, it can be considered a better approximation of the exact solution. The "$1h$" norm of the difference between the current solution $(\Omega_h, \{m_{\mathsf{P}}\})$ and the reference solution $(\Omega_{h+1/2}, \{m_{\mathsf{P}} + 1\})$ is used as global error estimate. Therefore, a comparison between the two solutions allows us to estimate the error on the less accurate of them, and decide which cells display the biggest approximation errors.

(*ii*) In the second step we decide whether an h or a p refinement must be performed on the actual approximation, that is the optimal refinement of each mesh cell P. Note that the $1h$ norm compares the univariate polynomial interpolation on each edge of each polygonal cell of the mesh. As we are comparing two solution obtained on

the actual mesh and a refined (and nested!) mesh, on each edge we compare the polynomial interpolation of degree m with two polynomial interpolations obtained using two sub-edges of degree $m+1$. The error due to the p-refinement is compared edge by edge with the error of the h refinement, and when the former is bigger than the latter a p-refinement the edge is marked for p refinement. When most of the edges of a given polygon are marked for p refinement, the h-refinement of that cell is switched off.

5.3. Test Case 1: the L-shaped domain. We consider the Poisson problem on an L-shaped domain, obtained carving out the lower right quarter from the square domain $[1,1]^2$. The source term f is zero everywhere, and the boundary conditions are set in accordance with the exact solution

$$u(r,\theta) = r^{2/3}\sin(2\theta/3)$$

here expressed in terms of the polar coordinates (r,θ) in the plane. The initial grid adopted in this test is given by applying the coordinate transformation mapping [15]

$$x = \xi + \phi\sin(2\pi\xi)\sin(2\pi\zeta)$$
$$y = \zeta + \phi\sin(2\pi\xi)\sin(2\pi\zeta)$$

with distortion parameter $\phi = 1$ to a regular grid of squares in the coordinates system (xi,ζ).

Although the load is regular, the exact solution u is only in $H^{5/3}(\Omega)$ due to the presence of the re-entrant corner. Thus, the expected asymptotic rates of convergence on uniformly refined meshes are $\mathsf{err} = \mathcal{O}(N^{-1/3})$. $\mathsf{err} = \mathcal{O}(N^{-m/2})$, which, for example, gives $\mathsf{err} = \mathcal{O}(N^{-1})$ for quadratic polynomials and $\mathsf{err} = \mathcal{O}(N^{-3/2})$ for cubic polynomials.

Figure 6.1 show that the numerical results agree with the theoretical predictions. Figure 6.2 shows the good behavior of the effectivity index. Figures 6.3-6.11 show how the adaptive strategy correctly refines near the re-entrant corner.

Figures 6.12-6.15 show the *hp*-adaptive strategy on a sequence of meshes of regular and distorted quadrilaterals. In the left column we show how the base mesh is refined and the values of the polynomial degree on each mesh edge in accordance with the following list: $m = 1$ (brown), $m = 2$ (blue), $m = 3$ (green), $m = 4$ (red).

5.4. Test Case 2: load with strong internal layer. In this test case, we consider the Poisson problem defined on the square domain $\Omega =]0,1[^2$ by setting the identity matrix for the diffusion tensor and choosing boundary conditions and right-hand side source term f consistent with the exact solution:

$$u(x,y) = 16x(1-x)y(1-y)\arctan(25x - 100y + 50), \qquad (x,y) \in \Omega.$$

The starting mesh for both uniformly and adaptively refined calculations is formed by hexagons built by a dualization procedure from a uniform triangle-based mesh.

As the exact solution u belongs to $H^2(\Omega)$ and the domain Ω, the asymptotic convergence rates of the numerical approximation on uniformly refined meshes, see Propositions 2.1 and 2.3, should be $err = \mathcal{O}(N^{1/2})$, since on such meshes the scaling $h = \mathcal{O}(N^{-1/2})$ holds. It is worth noting that the exact solution u is characterized by a region with a very strong gradient around the line of equation $y = 1/2 + x/4$.

Therefore, we expect that the numerical approximation to u attains the theoretical convergence rate only after that this internal layer has been resolved, i.e. once the size of the elements in this strong gradient region has become sufficiently small.

This implies a small value of the mesh size parameter h and thus a very large number of mesh elements N_{P} for the uniformly refined meshes.

Conversely, we expect the solutions obtained with the adaptive strategy to follow the theoretical rate in N also for rather coarse grids.

Figures 6.16-6.17 and 6.20-6.21 shows how the numerical results agree with the theoretical predictions. Figures 6.18-6.19 show the good behavior of the effectivity index. Figures 6.22-6.29 show how the adaptive strategy refines as expected in a neighborhood of this internal layer.

Figures 6.30-6.33 show the *hp*-adaptive strategy on a sequence of meshes of regular and distorted quadrilaterals. In the left column we show how the base mesh is refined and the values of the polynomial degree on each mesh edge in accordance with the following list: $m = 1$ (brown), $m = 2$ (blue), $m = 3$ (green), $m = 4$ (red).

6. Conclusions. A posteriori error estimation and adaptivity were presented in the context of mimetic and virtual element methods, which exploit the mesh flexibility of such schemes. The challenge in this work is that the lack of knowledge of the basis functions makes the development of error estimators not straightforward. A residual based a posteriori error estimator for the virtual element method introduced in [4] was proposed, that immediately applies also to its mimetic counterpart. The reliability of the estimator was theoretically proved and performance in combination with an adaptive strategy investigated numerically.

Acknowledgements

The work of the second author was partially supported by the National Nuclear Security Administration of the U.S. Department of Energy at Los Alamos National Laboratory under Contract No. DE-AC52-06NA25396 and the DOE Office of Science Advanced Scientific Computing Research (ASCR) Program in Applied Mathematics.

REFERENCES

[1] M. Ainsworth and J. T. Oden. A posteriori error estimation in finite element analysis. *Comput. Methods Appl. Mech. Engrg.*, 142(1-2):1–88, 1997.

[2] P.F. Antonietti, L. Beirão da Veiga, C. Lovadina, and M. Verani. Hierarchical a posteriori error estimators for the mimetic discretization of elliptic problems. Technical report.

[3] L. Beirão da Veiga. A residual based error estimator for the mimetic finite difference method. *Numer. Math.*, 108(3):387–406, 2008.

[4] L. Beirão da Veiga, F. Brezzi, A. Cangiani, G. Manzini, L. D. Marini, and A. Russo. The Virtual Element Method. *Math. Models Methods Appl. Sci.*, 2013. (to appear).

[5] L. Beirão da Veiga, F. Brezzi, and L. D. Marini. Virtual Elements for linear elasticity problems. Technical Report Preprint IMATI 11cPV12/10/0, IMATI-CNR, 2011. (submitted for publication).

[6] L. Beirão da Veiga, K. Lipnikov, and G. Manzini. Arbitrary-order nodal mimetic discretizations of elliptic problems on polygonal meshes. *SIAM Journal on Numerical Analysis*, 49(5):1737–1760, 2011.

[7] L. Beirão da Veiga and G. Manzini. An a posteriori error estimator for the mimetic finite difference approximation of elliptic problems. *Int. J. Numer. Meth. Engrg.*, 76(11):1696–1723, 2008.

[8] L. Beirão da Veiga and G. Manzini. A higher-order formulation of the mimetic finite difference method. *SIAM Journal on Scientific Computing*, 31(1):732–760, 2008.

[9] L. Beirão da Veiga and G. Manzini. The mimetic finite difference method and the virtual element method for elliptic problems with arbitrary regularity. Technical Report LA-UR, Los Alamos National Laboratory, 2012. submitted for publication to IMA J. Numer. Anal.

[10] D. Braess. *Finite elements. Theory, fast solvers, and applications in elasticity theory.* Cambridge University Press, third edition, 2007.

[11] S. Brenner and L. Scott. *The Mathematical Theory of Finite Element Methods*. Springer-Verlag, Berlin/Heidelberg, 1994.

[12] F. Brezzi, A. Buffa, and K. Lipnikov. Mimetic finite differences for elliptic problems. *M2AN Math. Model. Numer. Anal.*, 43(2):277–295, 2009.

[13] F. Brezzi and M. Fortin. *Mixed and Hybrid Finite Element Methods*. Springer-Verlag, New York, 1991.

[14] F. Brezzi, K. Lipnikov, and M. Shashkov. Convergence of the mimetic finite difference method for diffusion problems on polyhedral meshes. *SIAM J. Numer. Anal.*, 43(5):1872–1896, 2005.

[15] F. Brezzi, K. Lipnikov, M Shashkov, and V. Simoncini. A new discretization methodology for diffusion problems on generalized polyhedral meshes. *Comput. Methods Appl. Mech. Engrg.*, 196:3682–3692, 2007.

[16] F. Brezzi, K. Lipnikov, and V. Simoncini. A family of mimetic finite difference methods on polygonal and polyhedral meshes. *Math. Models Methods Appl. Sci.*, 15(10):1533–1551, 2005.

[17] P. G. Ciarlet. *The Finite Element Method for Elliptic Problems*. North-Holland, Amsterdam, 1978.

[18] P.G. Ciarlet. *The finite element method for elliptic problems*. North-Holland, Amsterdam, 1978.

[19] L. Demkowicz. *Computing with $h-p$ finite elements*, volume 1. One and two-dimensional elliptic and Maxwell problems. Chapman&Hall/CRC, Boca Raton, Florida, 2007.

[20] L. Demkowicz, W. Rachovicz, and Ph. Devloo. A fully automatics $h-p$ adaptivity. *J. Sci. Comput.*, 17:127–155, 2002.

[21] P. Grisvard. *Elliptic problems in nonsmooth domains*, volume 24 of *Monographs and Studies in Mathematics*. Pitman, Boston, 1985.

[22] T. J. R. Hughes. *The finite element method. Linear static and dynamic finite element analysis*. Dover, second edition, 2000.

[23] J. M. Melenk and B. I. Wohlmuth. On residual-based a posteriori error estimation in *hp*-fem. *Adv. Comput. Math.*, 15:311–331, 2001.

[24] A. Patra and A. Gupta. A systematic strategy for simultaneous adaptive $h-p$ finite element mesh modiifcation using non-linear programming. *Comput. Methods Appl. Mech. Engrg.*, 190:3797–3818, 2001.

[25] W. Rachovicz, T. Oden, and L. Demkowicz. Toward a universal $h-p$ adaptive finite element strategy. Part 3. Design of $h-p$ meshes. *Comput. Methods Appl. Mech. Engrg.*, 77:181–212, 1989.

[26] R. Verfürth. *A review of a posteriori error estimation and adaptive mesh refinement*. Wiley and Teubner, Stuttgart, 1996.

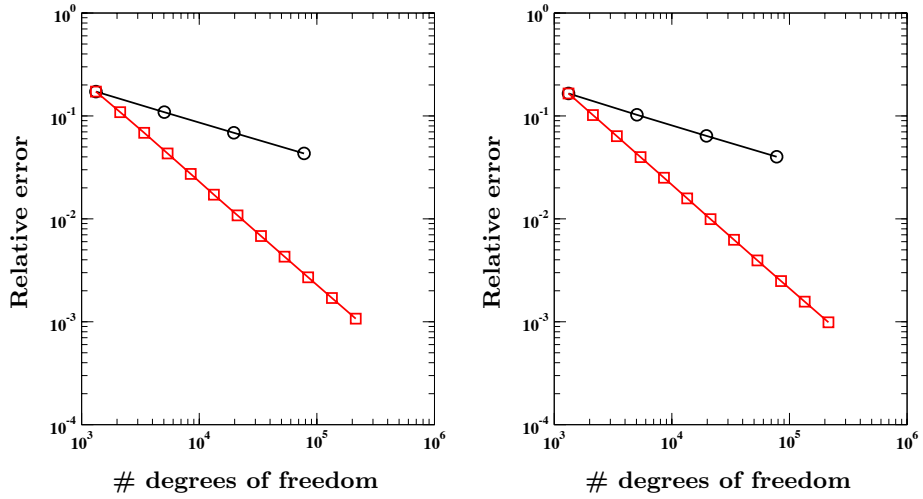

FIG. 6.1. *Test 1. Relative error curves: regular quadrilateral mesh (left), distorted quadrilateral mesh (right); uniform refinement (black circles), adaptive refinement (red squares).*

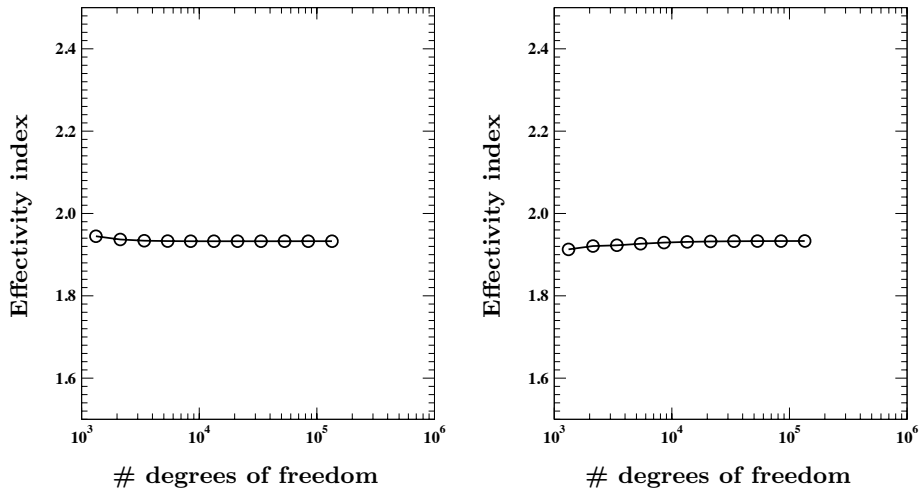

FIG. 6.2. *Test 1. Effectivity index: regular quadrilateral mesh (left), distorted quadrilateral mesh (right).*

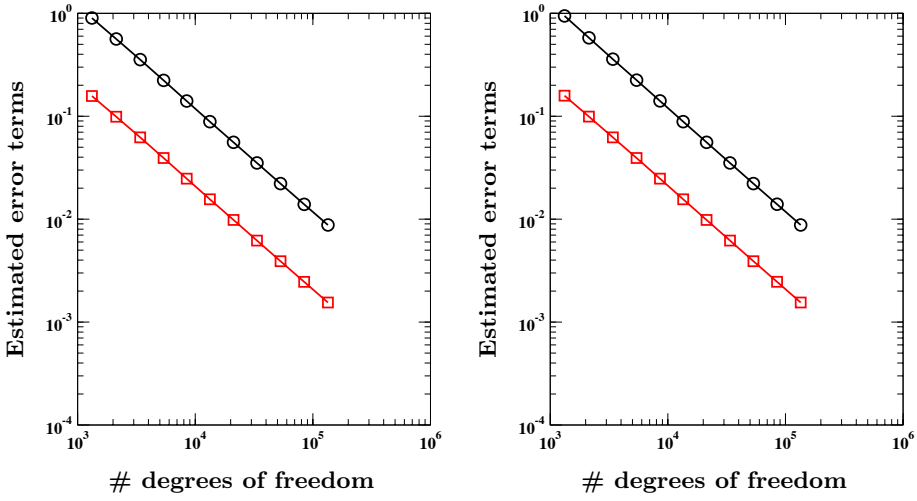

FIG. 6.3. *Test 1. Estimated error terms, projected Laplace operator (circles), stability term (squares): regular quadrilateral mesh (left), distorted quadrilateral mesh (right).*

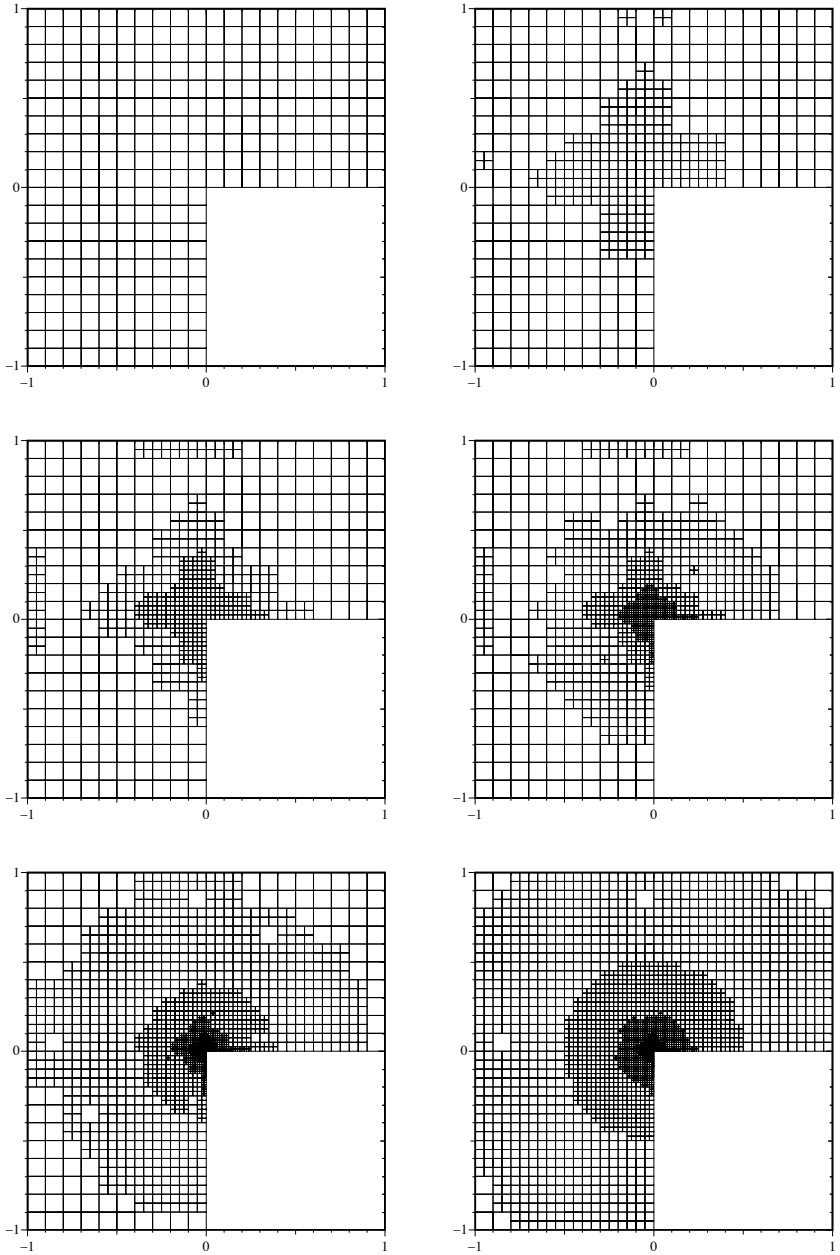

FIG. 6.4. *Test 1. Regular quadrilateral mesh, refinements 0-5*

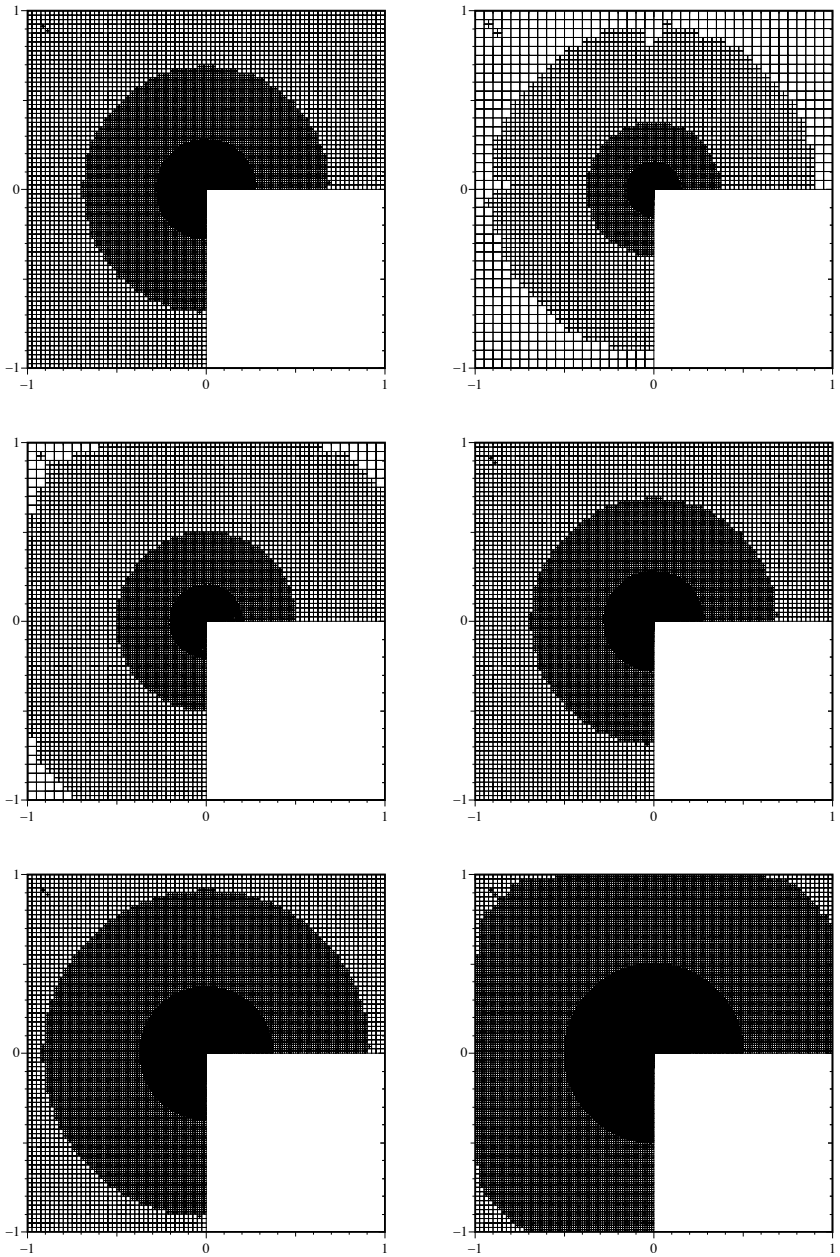

FIG. 6.5. *Test 1. Regular quadrilateral mesh, refinements 6-11*

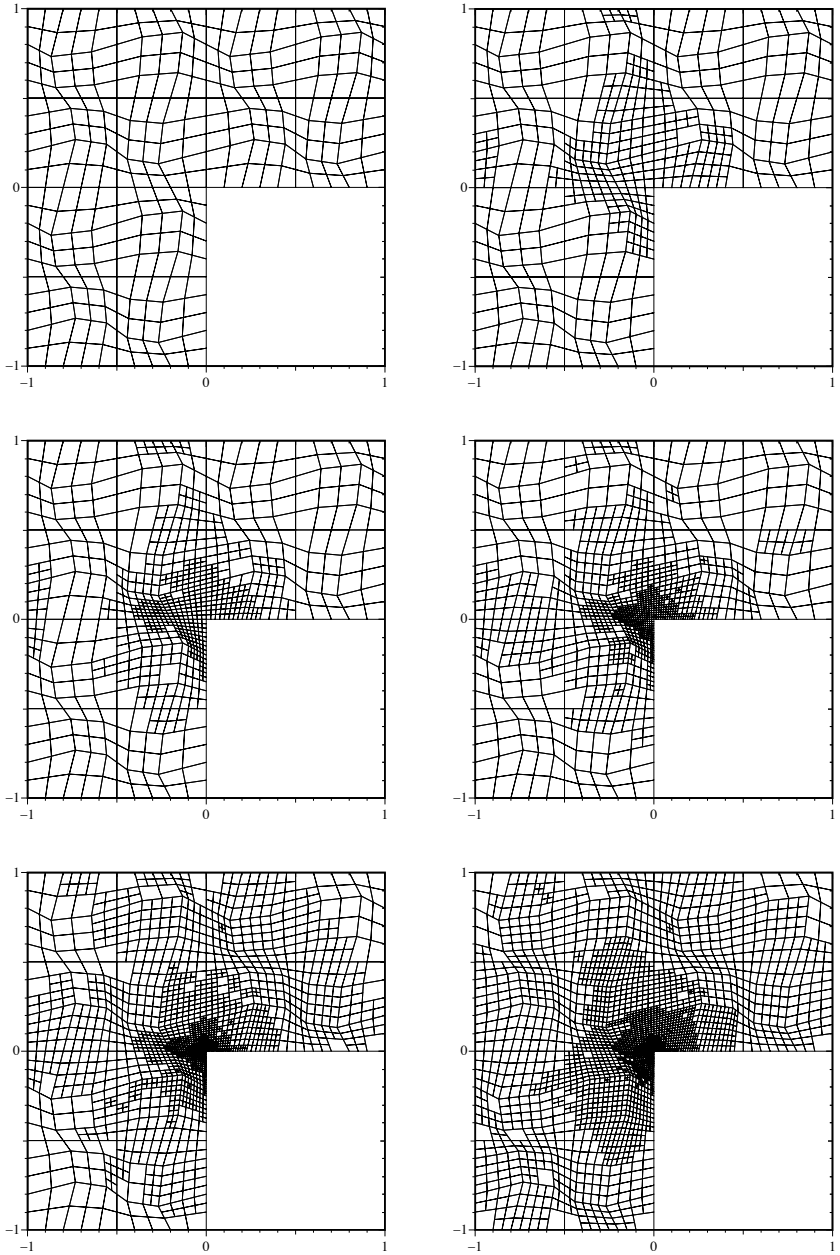

FIG. 6.6. *Test 1. Distorted quadrilateral mesh, refinements 0-5*

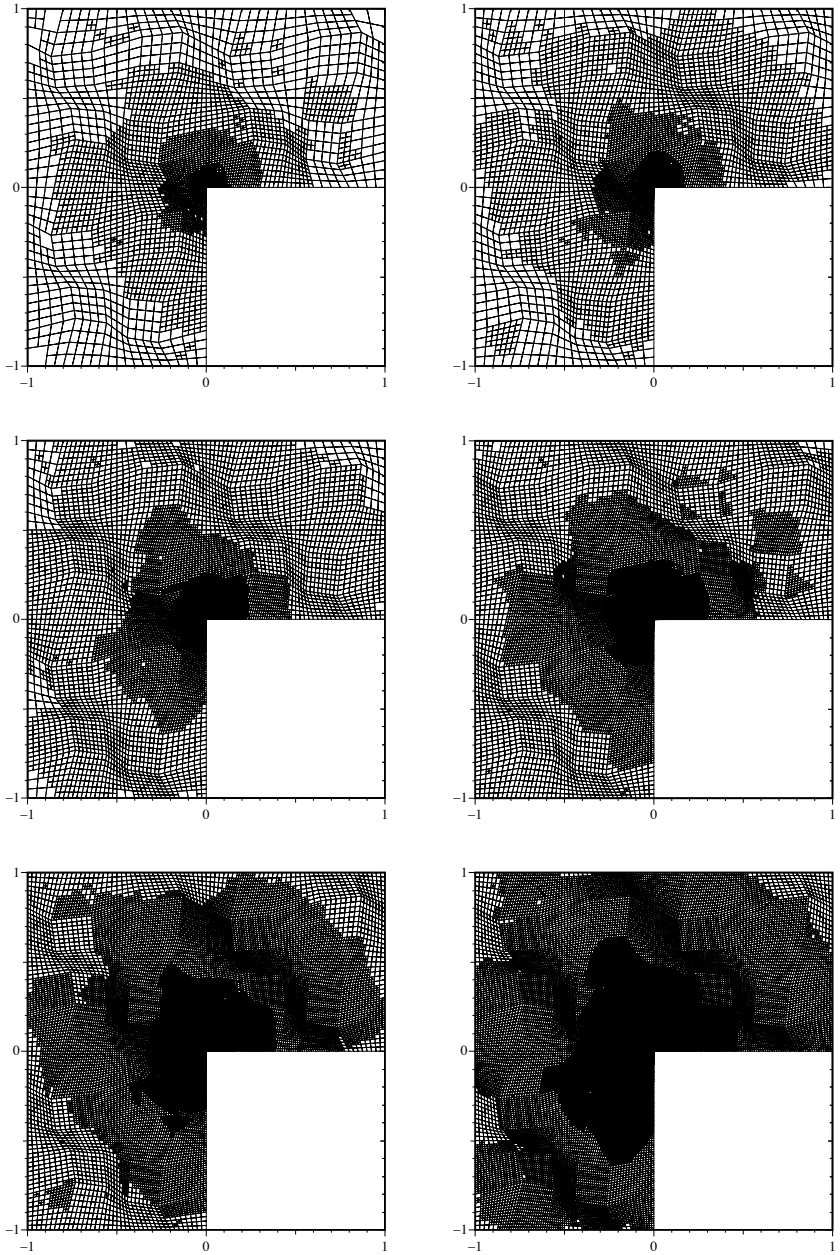

FIG. 6.7. *Test 1. Distorted quadrilateral mesh, refinements 6-11*

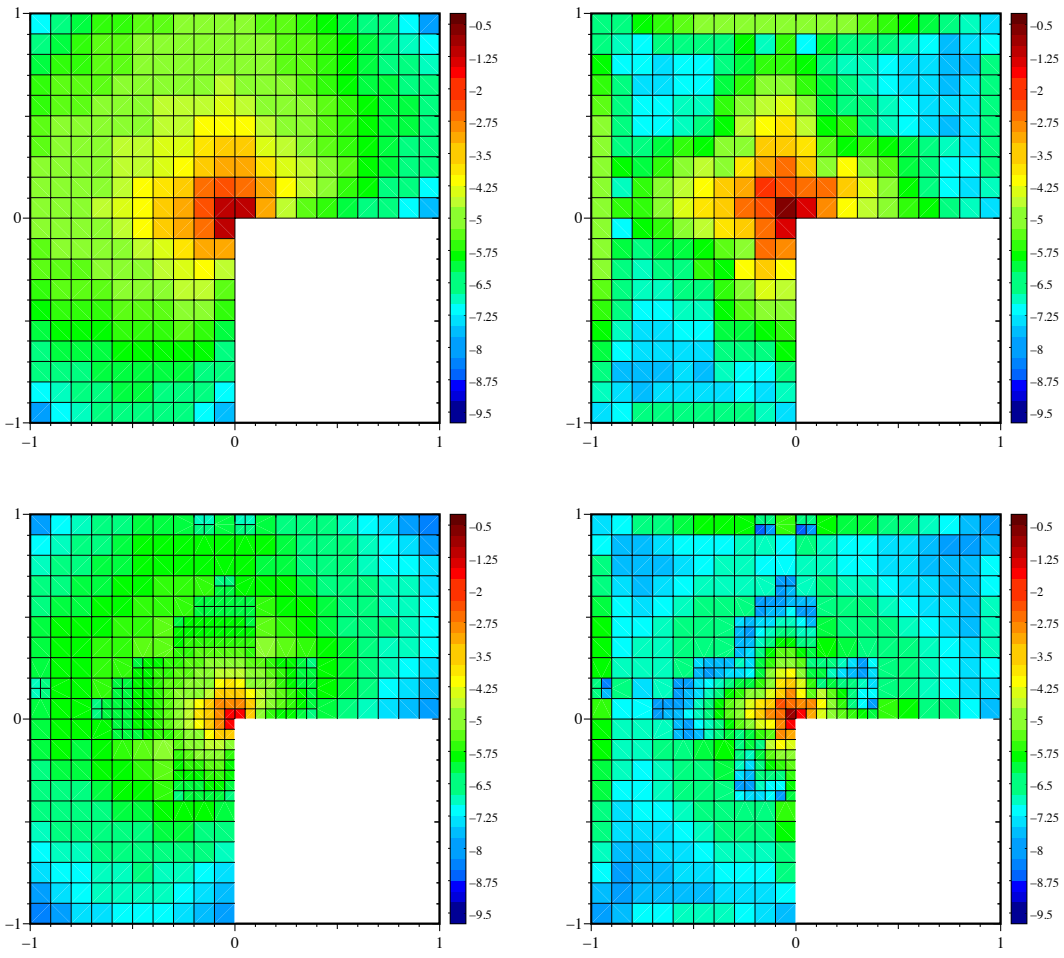

FIG. 6.8. *Test 1. Refinements 0 (top) and 1 (bottom). Absolute error (left) and half of the estimated error (right)*

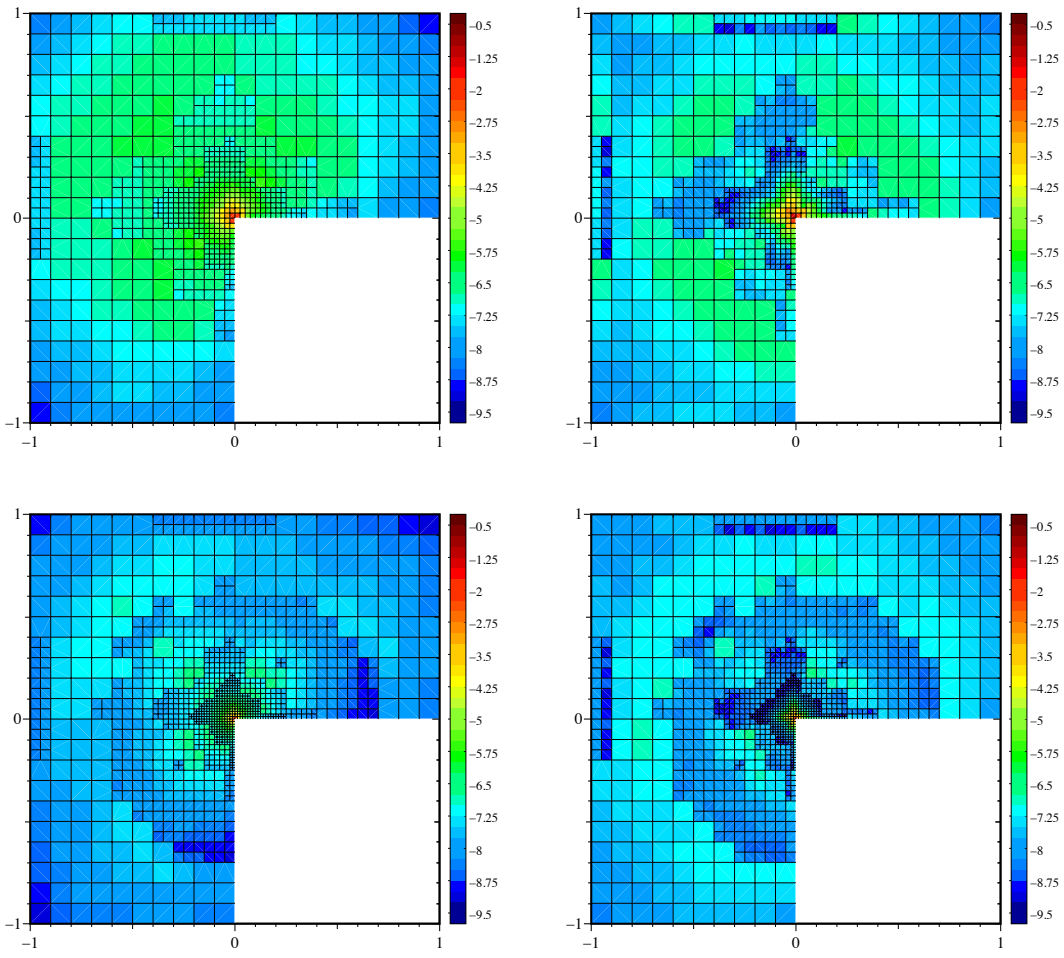

FIG. 6.9. *Test 1. Refinements 2 (top) and 3 (bottom). Absolute error (left) and half of the estimated error (right)*

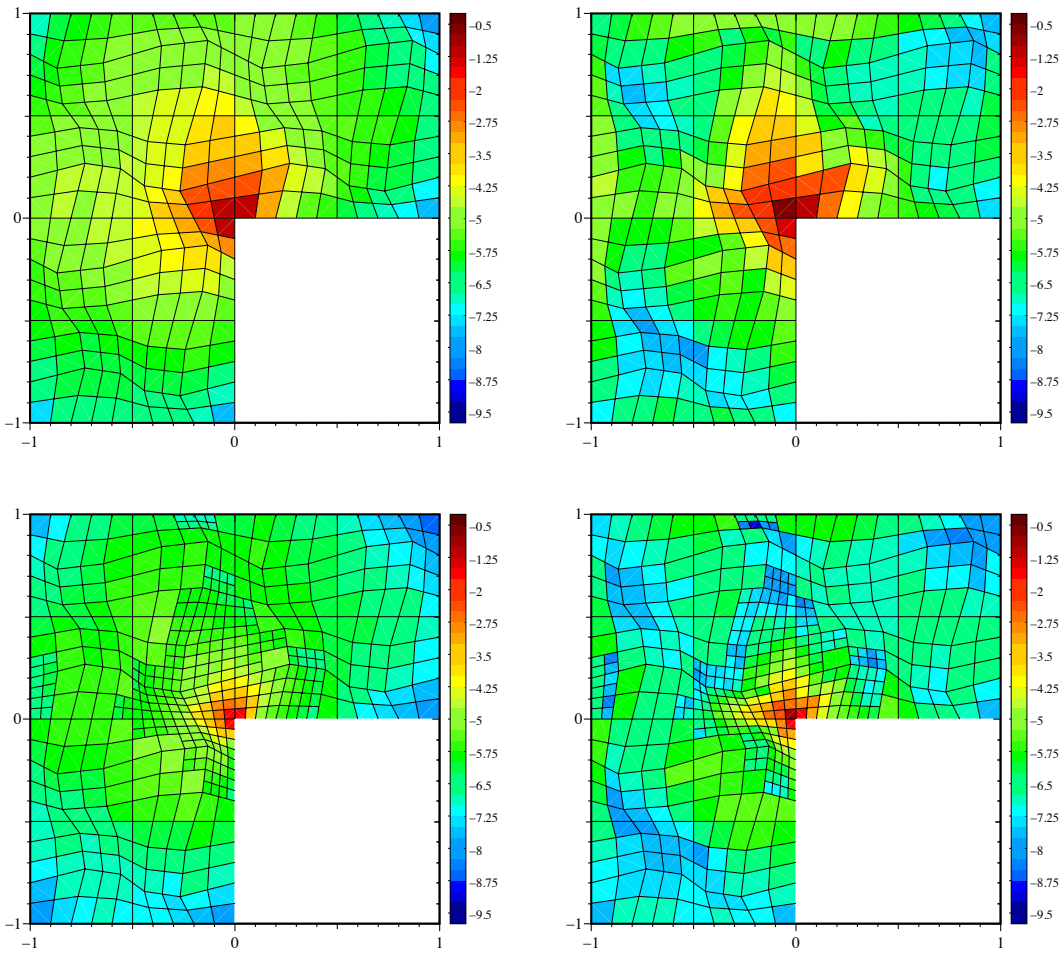

FIG. 6.10. *Test 1. Refinements 0 (top) and 1 (bottom). Absolute error (left) and half of the estimated error (right)*

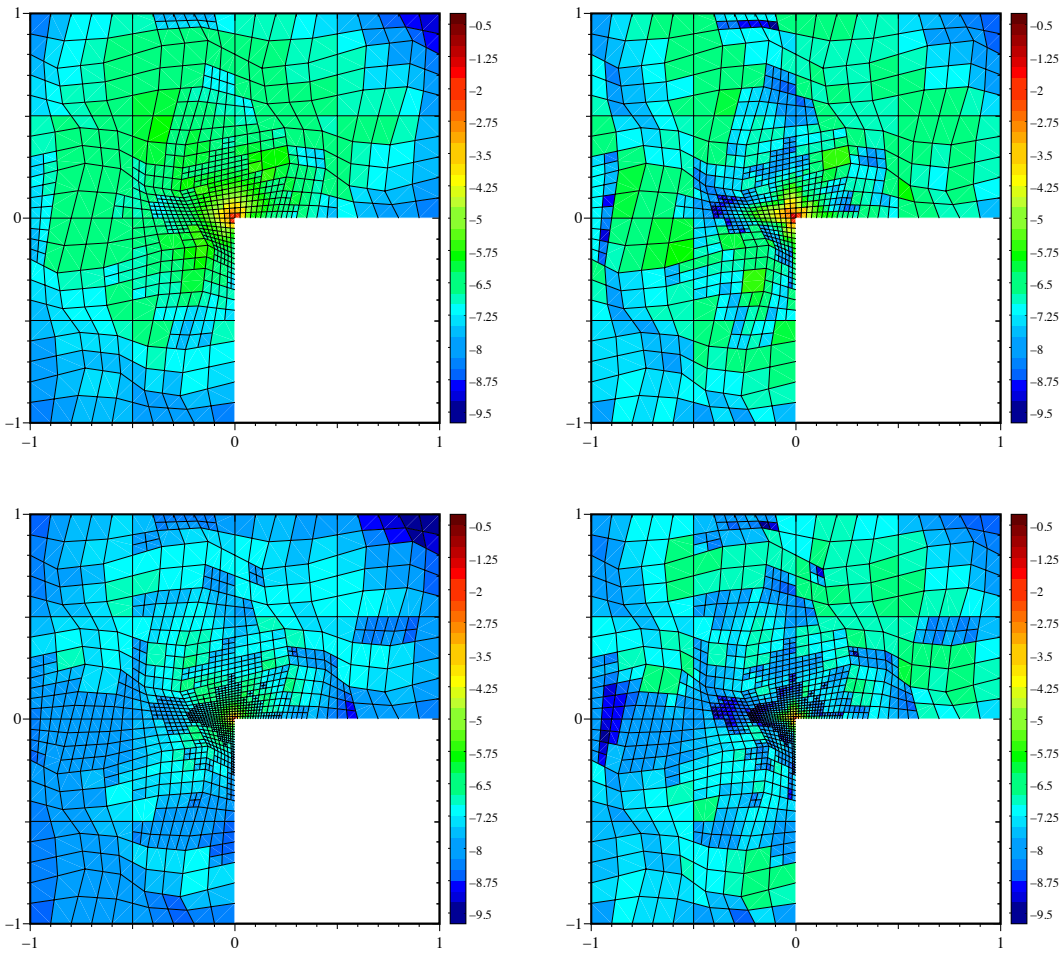

FIG. 6.11. *Test 1. Refinements 2 (top) and 3 (bottom). Absolute error (left) and half of the estimated error (right)*

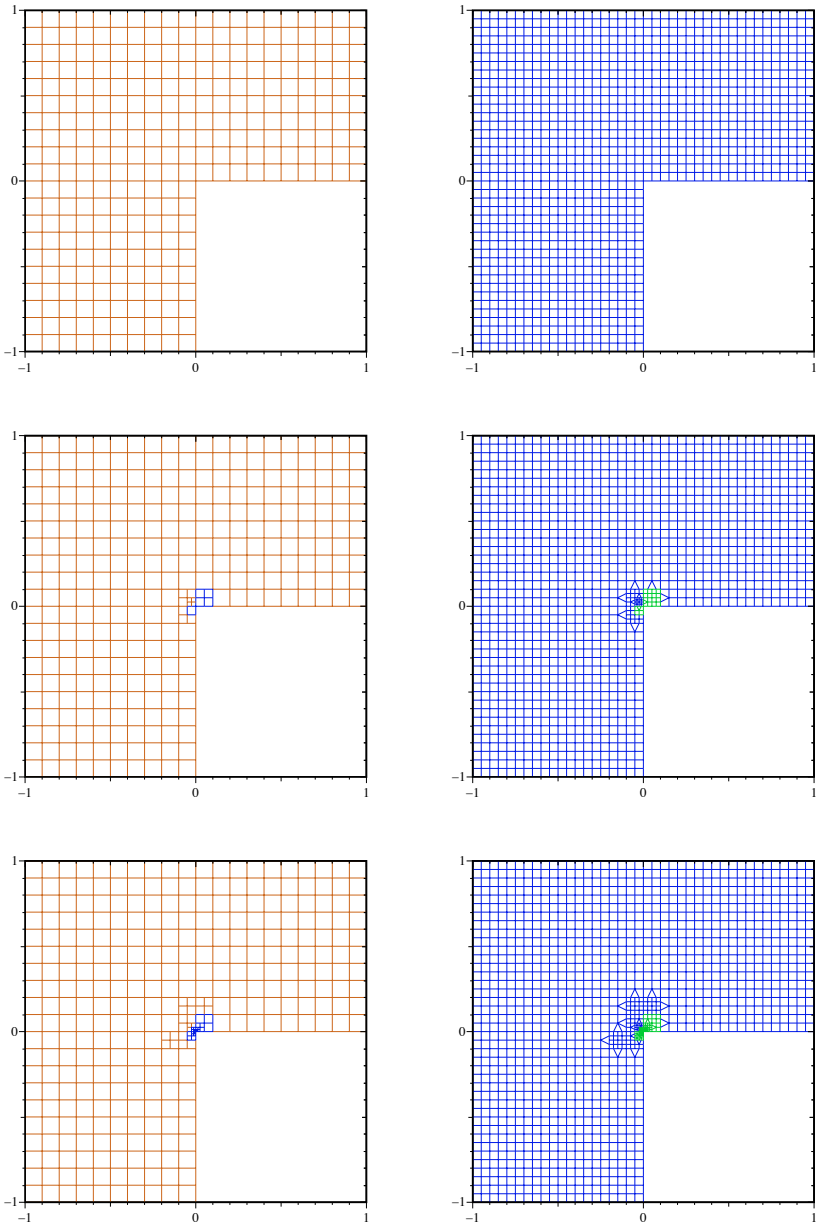

FIG. 6.12. *Test 1. Regular quadrilateral mesh; hp-refinements 0, 3, 6 on the base mesh (left) and on the reference mesh (right); $m = 1$ (brown), $m = 2$ (blue), $m = 3$ (green), $m = 4$ (red).*

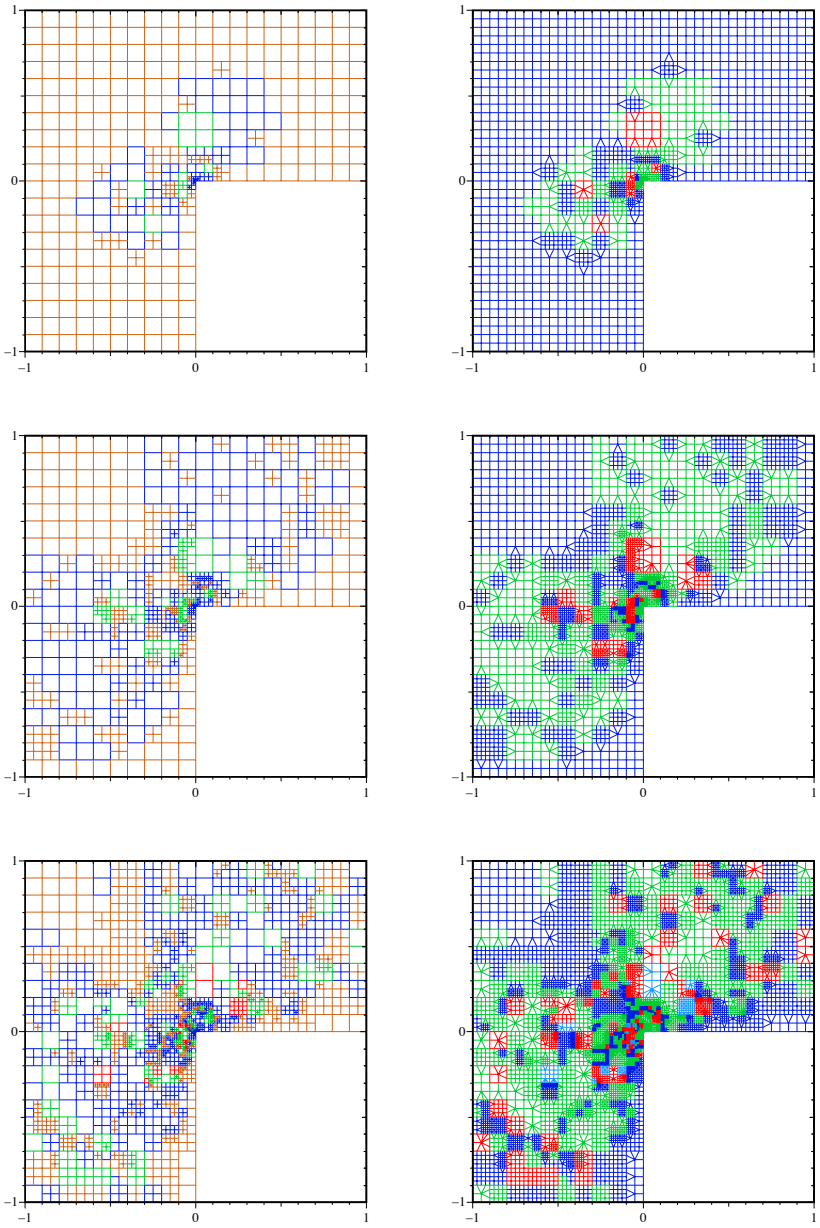

FIG. 6.13. *Test 1. Regular quadrilateral mesh; hp-refinements 9, 12, 15 on the base mesh (left) and on the reference mesh (right);* $m = 1$ *(brown),* $m = 2$ *(blue),* $m = 3$ *(green),* $m = 4$ *(red).*

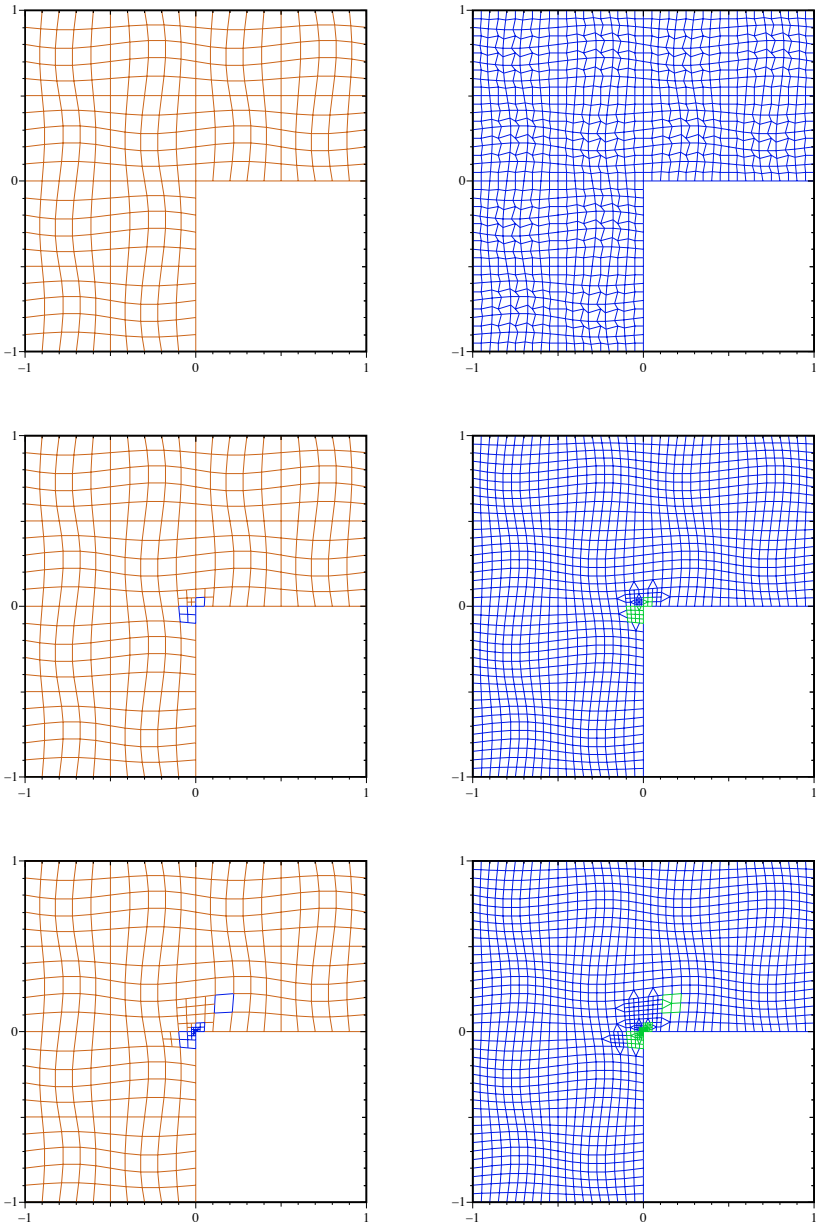

FIG. 6.14. *Test 1. Distorted quadrilateral mesh; hp-refinements 0, 3, 6 on the base mesh (left) and on the reference mesh (right);* $m = 1$ *(brown),* $m = 2$ *(blue),* $m = 3$ *(green),* $m = 4$ *(red).*

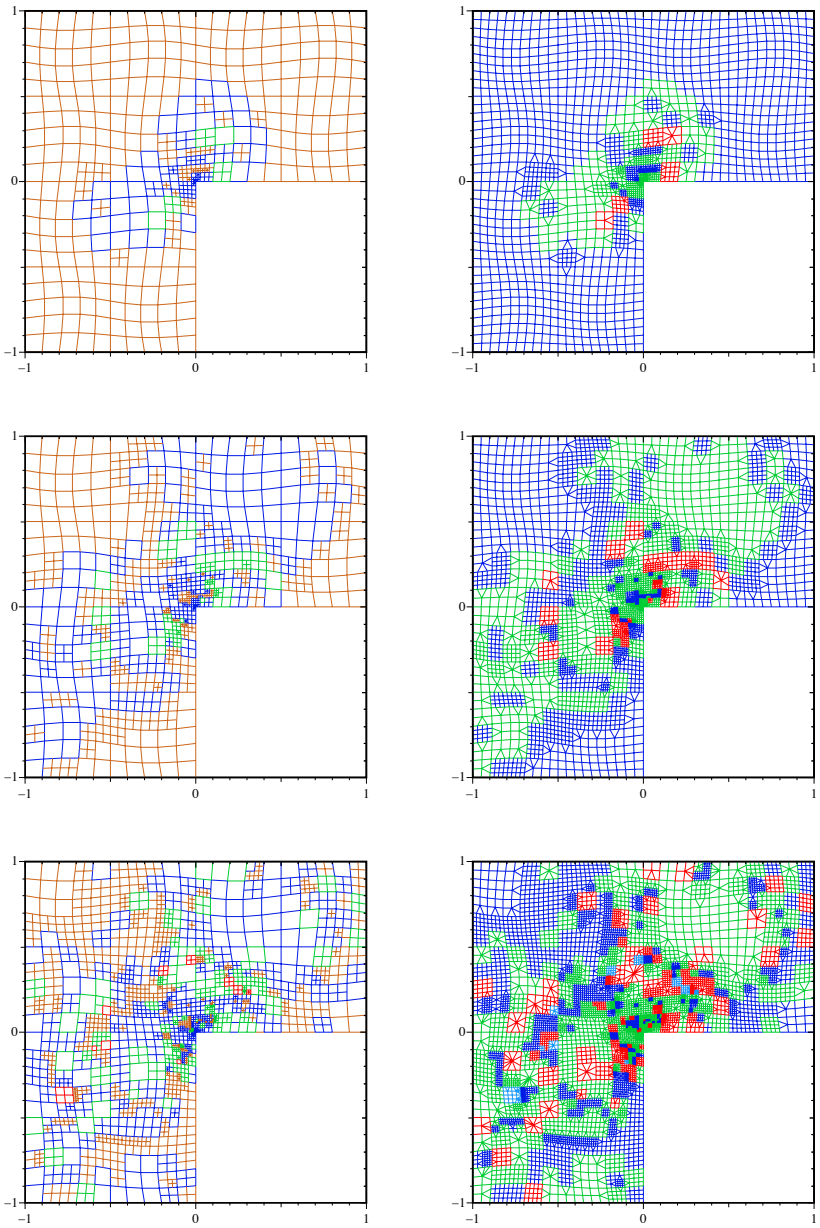

FIG. 6.15. *Test 1. Distorted quadrilateral mesh; hp-refinements 9, 12, 15 on the base mesh (left) and on the reference mesh (right);* $m = 1$ *(brown),* $m = 2$ *(blue),* $m = 3$ *(green),* $m = 4$ *(red).*

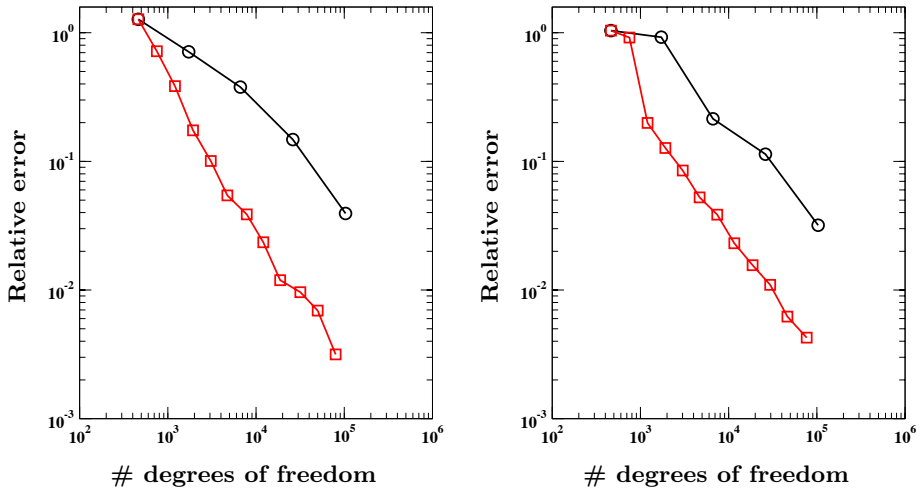

FIG. 6.16. *Test 2. Relative error curves: regular quadrilateral mesh (left), distorted quadrilateral mesh (right); uniform refinement (black circles), adaptive refinement (red squares).*

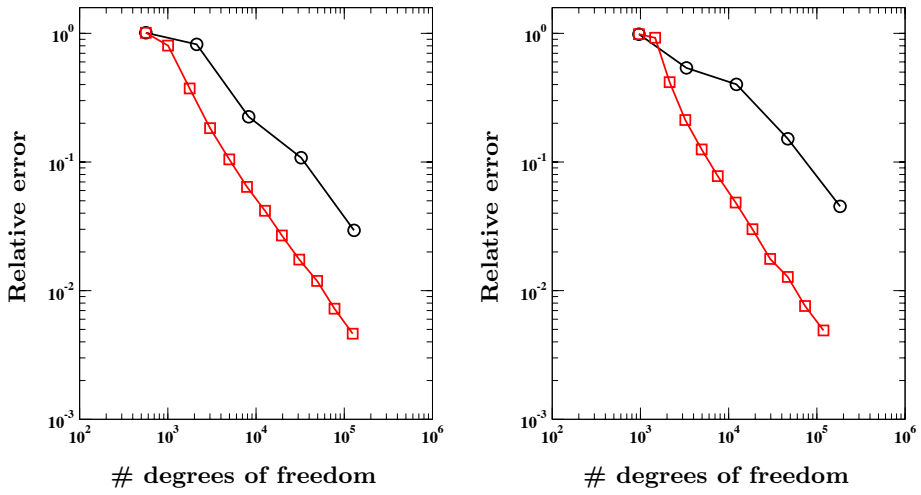

FIG. 6.17. *Test 2. Relative error curves: distorted triangular mesh mesh (left), mainly hexagonal mesh (right); uniform refinement (black circles), adaptive refinement (red squares).*

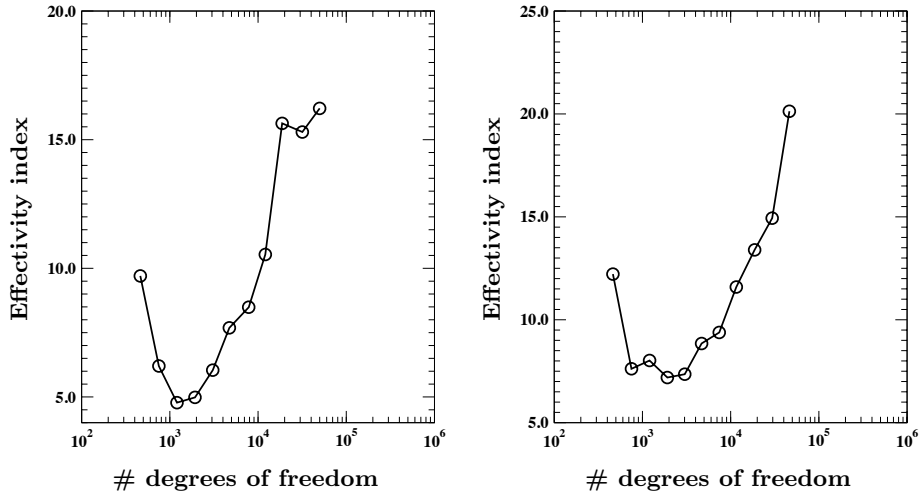

FIG. 6.18. *Test 2. Effectivity index: regular quadrilateral mesh (left), distorted quadrilateral mesh (right).*

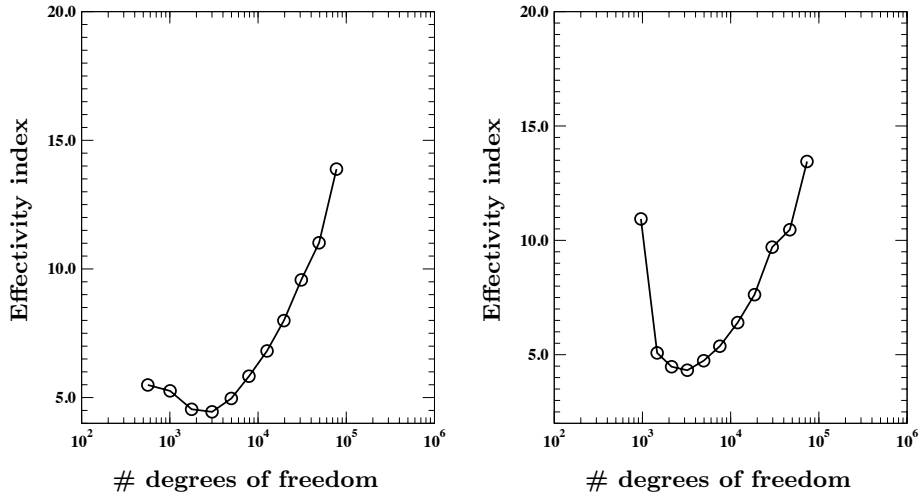

FIG. 6.19. *Test 2. Effectivity index: distorted triangular mesh (left), mainly hexagonal mesh (right).*

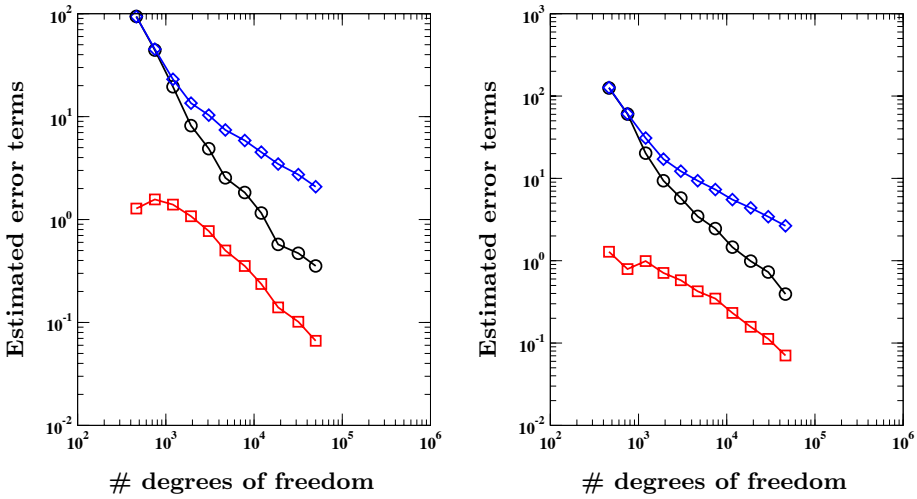

FIG. 6.20. *Test 2. Estimated error terms, projected Laplace operator (circles), stability term (squares), load term (diamonds) : regular quadrilateral mesh (left), distorted quadrilateral mesh (right).*

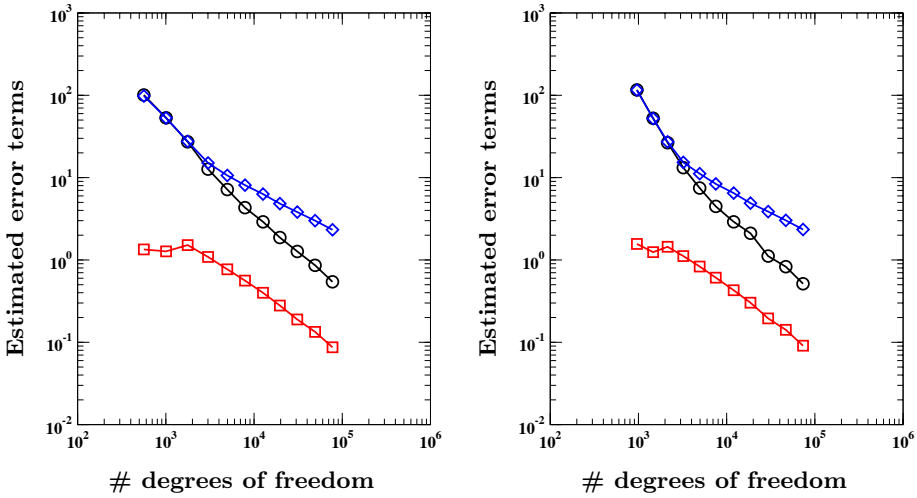

FIG. 6.21. *Test 2. Estimated error terms, projected Laplace operator (circles), stability term (squares), load term (diamonds) : distorted triangular mesh (left), mainly hexagonal mesh (right).*

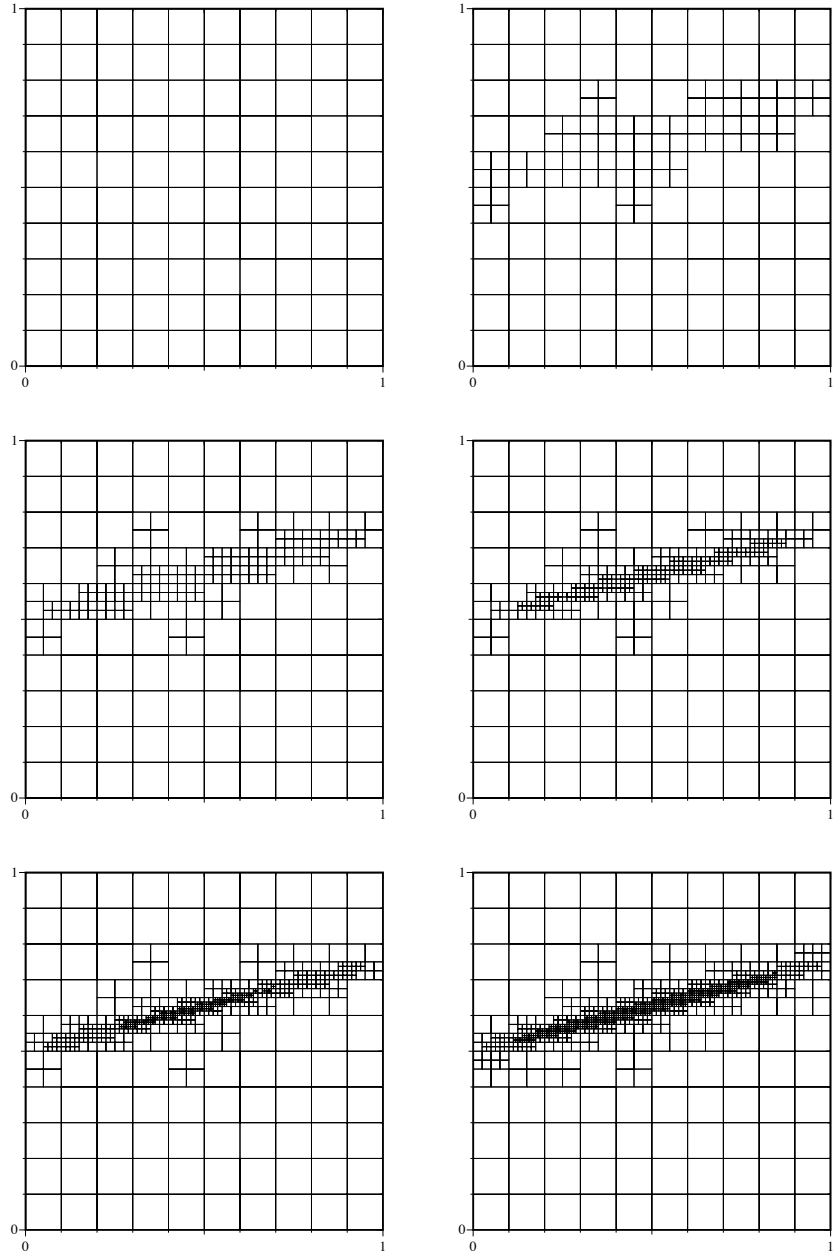

FIG. 6.22. *Test 2. Regular quadrilateral mesh, refinements 0-5*

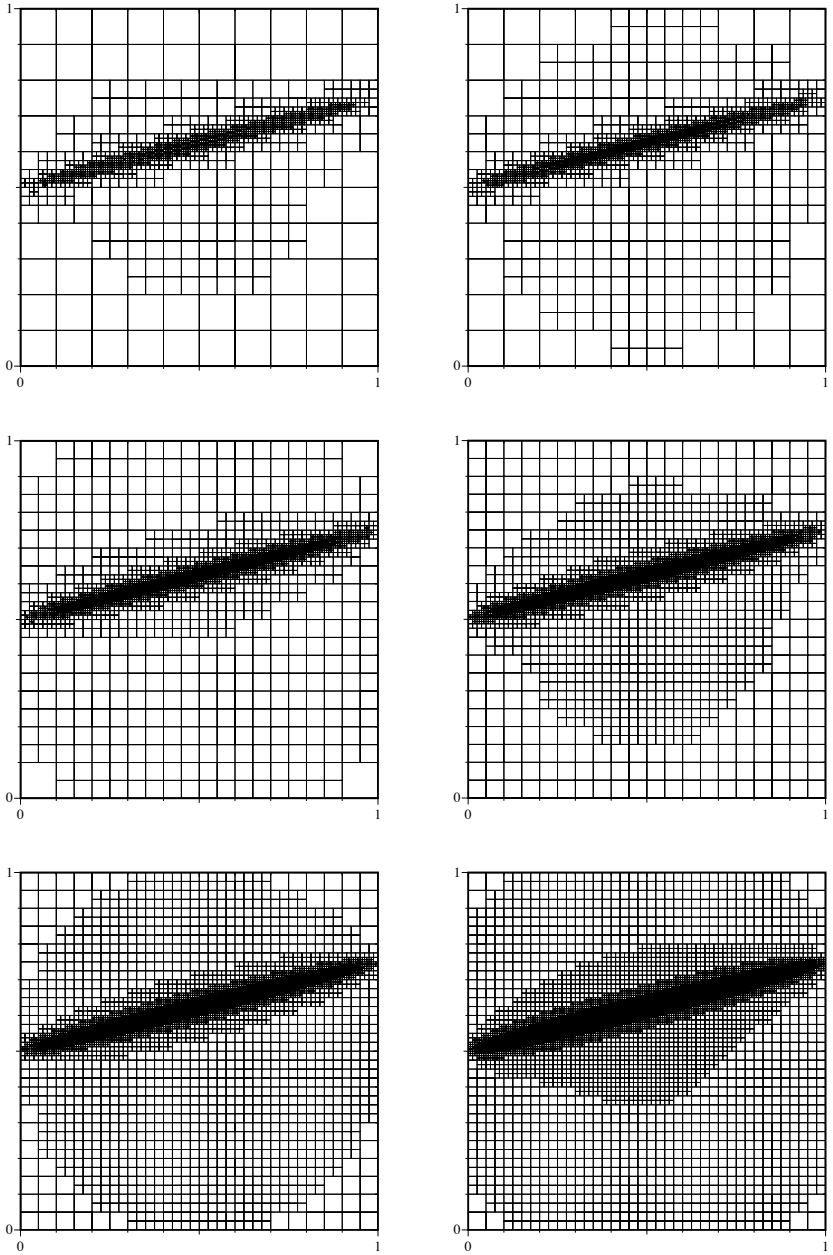

FIG. 6.23. *Test 2. Regular quadrilateral mesh, refinements 6-11*

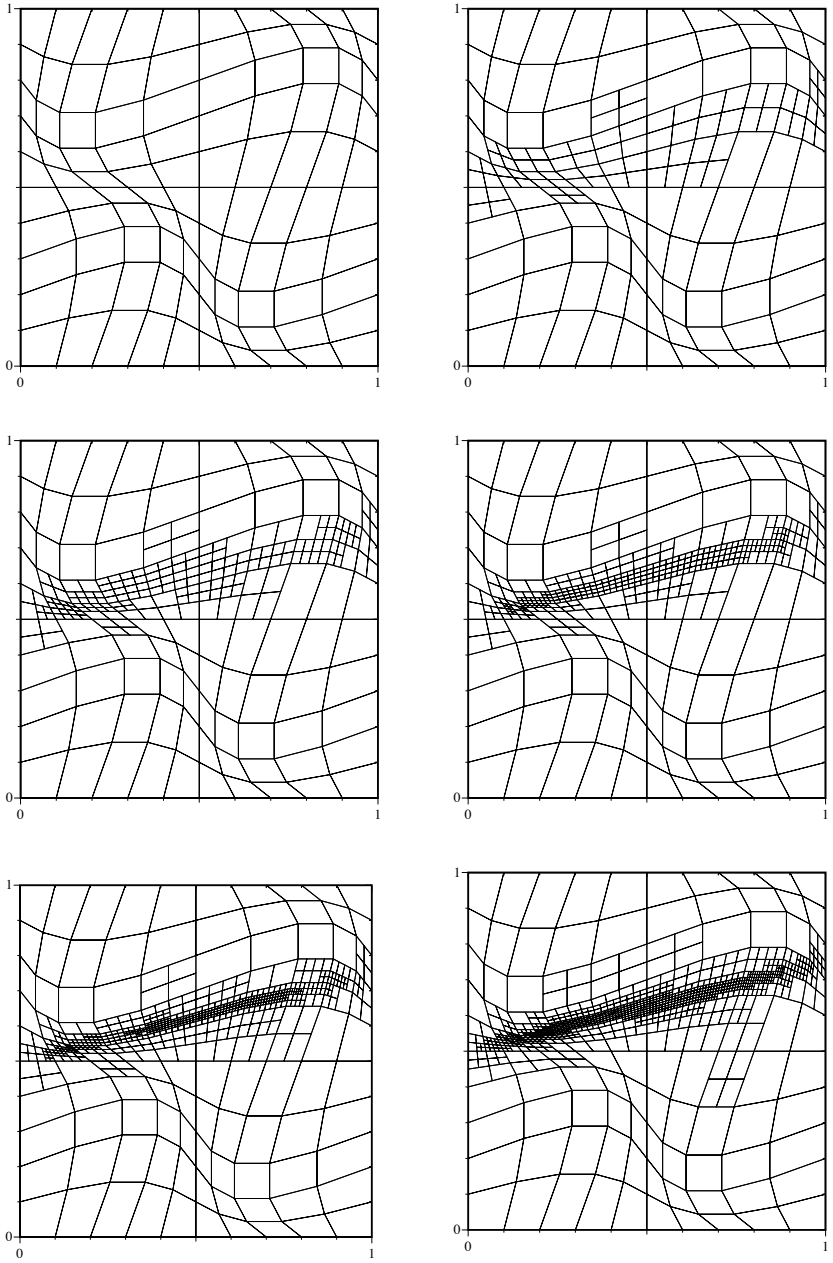

FIG. 6.24. *Test 2. Distorted quadrilateral mesh, refinements 0-5*

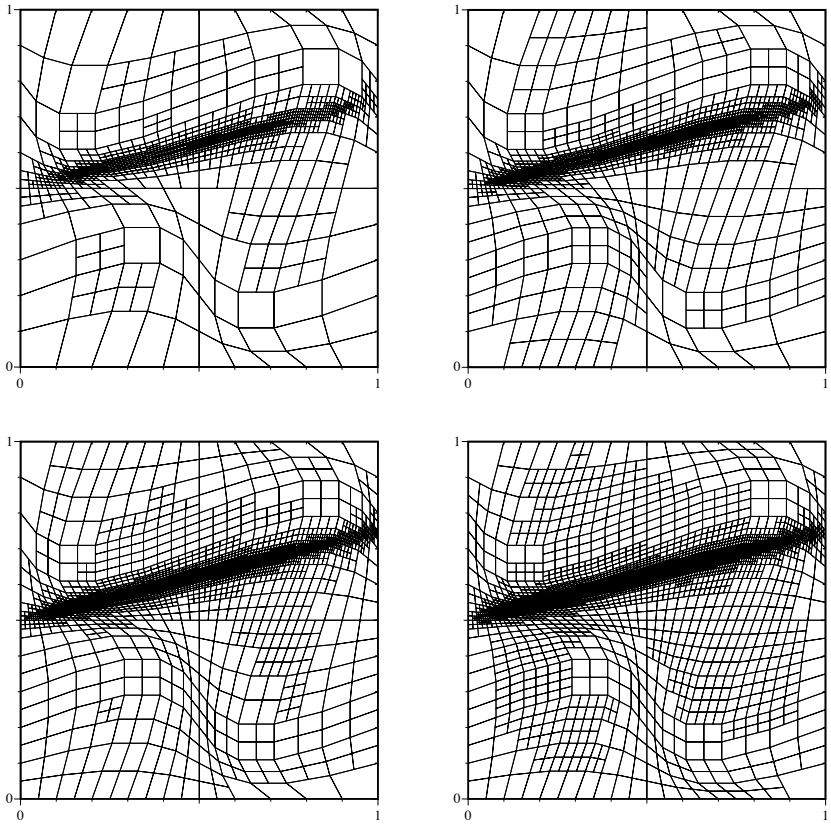

FIG. 6.25. *Test 2. Distorted quadrilateral mesh, refinements 6-11*

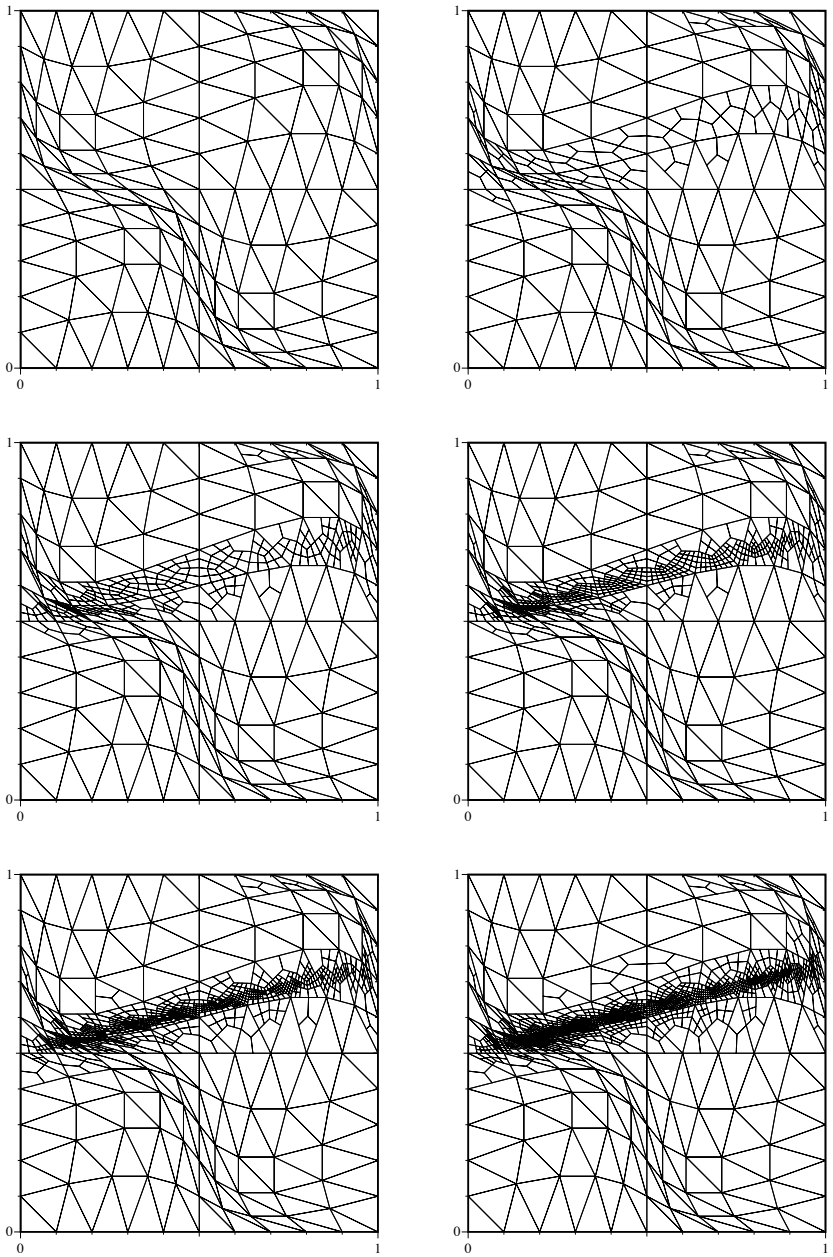

FIG. 6.26. *Test 2. Distorted triangular mesh, refinements 0-5*

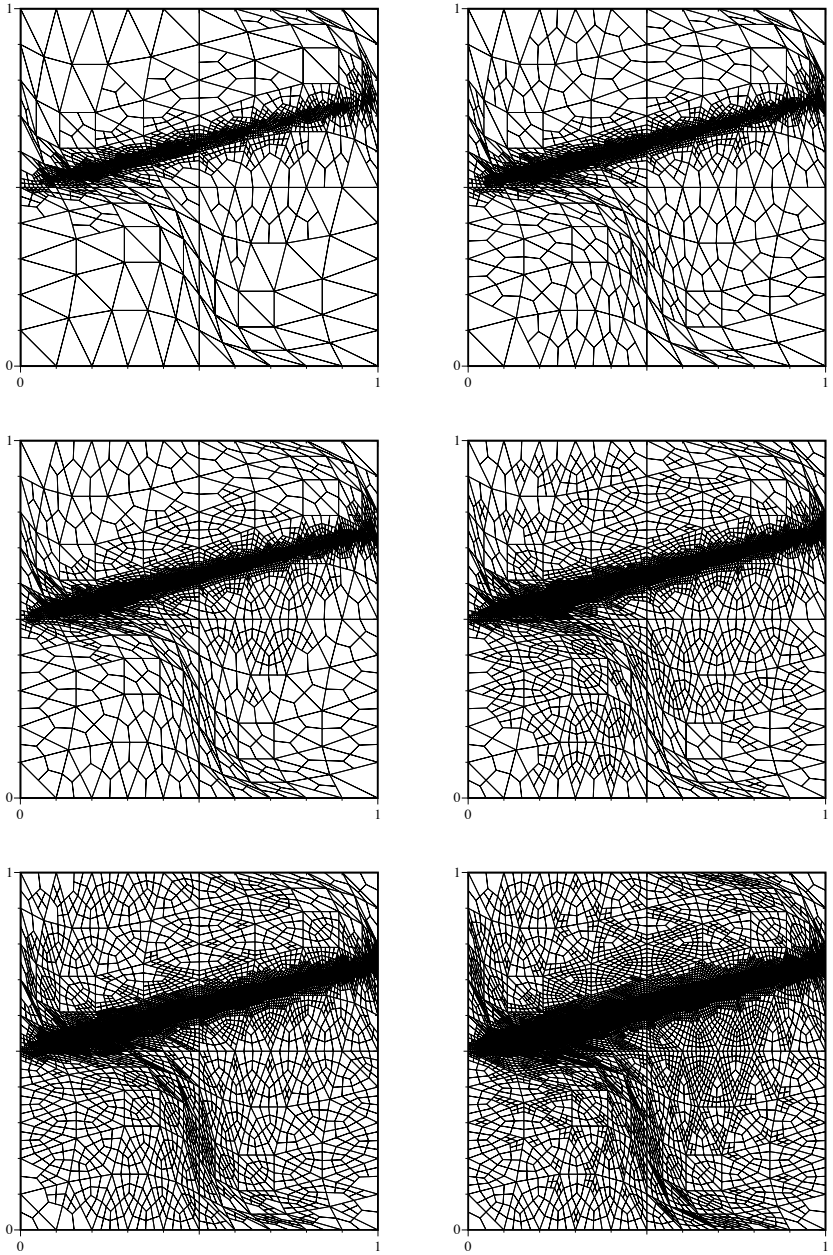

FIG. 6.27. *Test 2. Distorted triangular mesh, refinements 6-11*

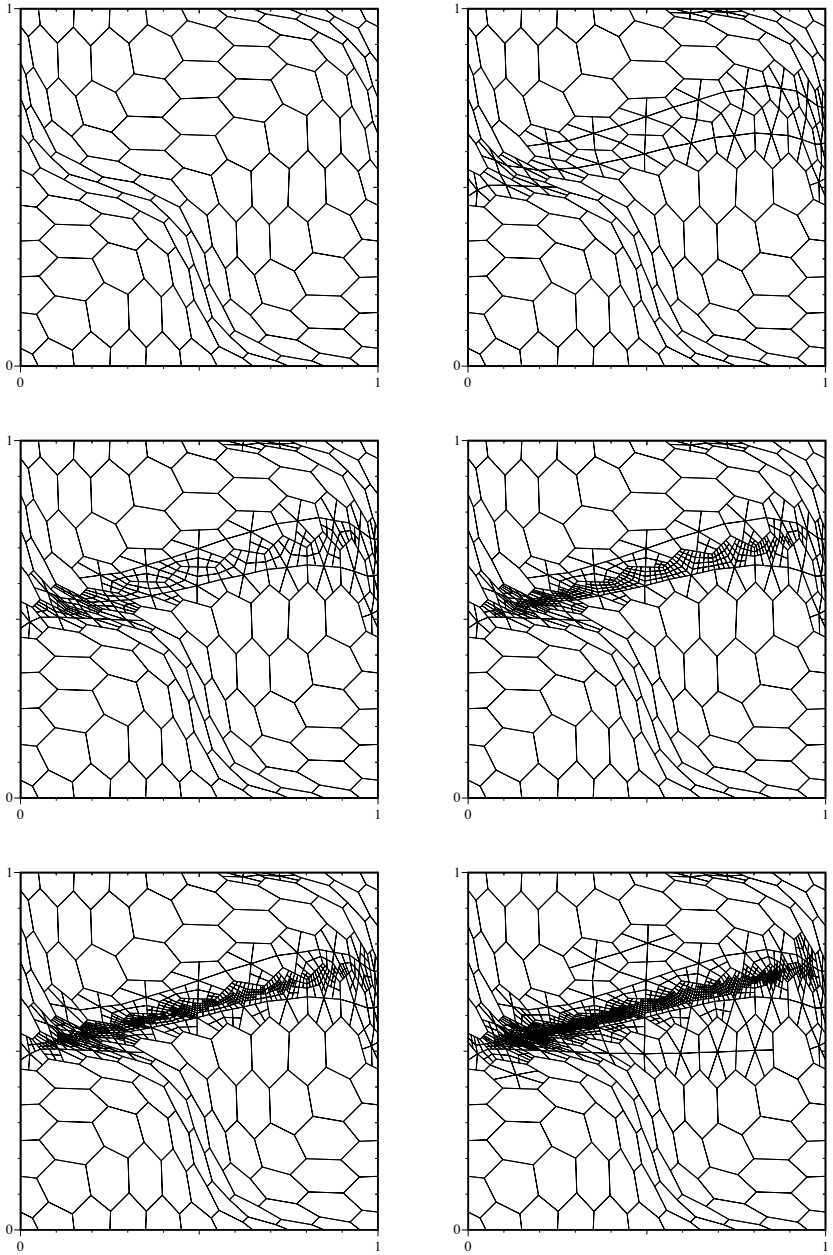

FIG. 6.28. *Test 2. Mainly hexagonal mesh, refinements 0-5*

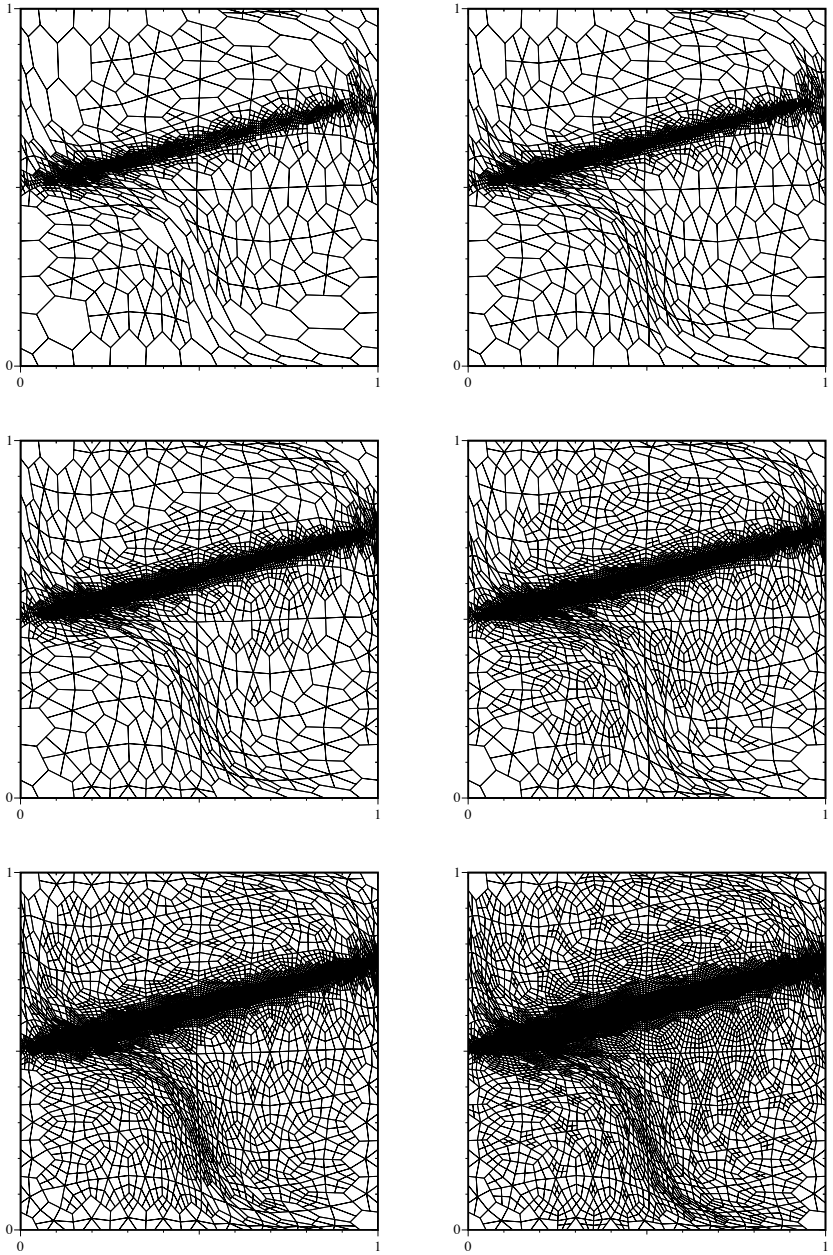

FIG. 6.29. *Test 2. Mainly hexagonal mesh, refinements 6-11*

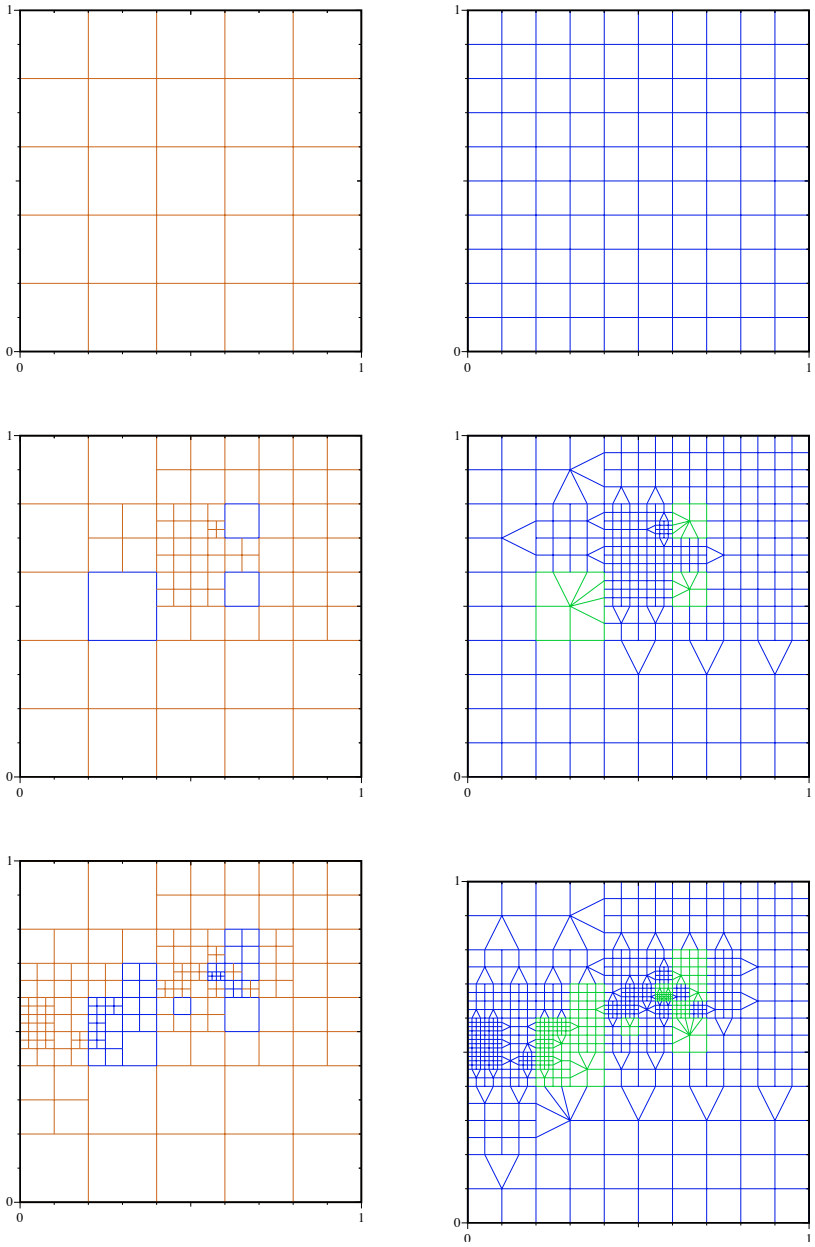

FIG. 6.30. *Test 2. Regular quadrilateral mesh; hp-refinements 0, 3, 6 on the base mesh (left) and on the reference mesh (right);* $m = 1$ *(brown),* $m = 2$ *(blue),* $m = 3$ *(green),* $m = 4$ *(red).*

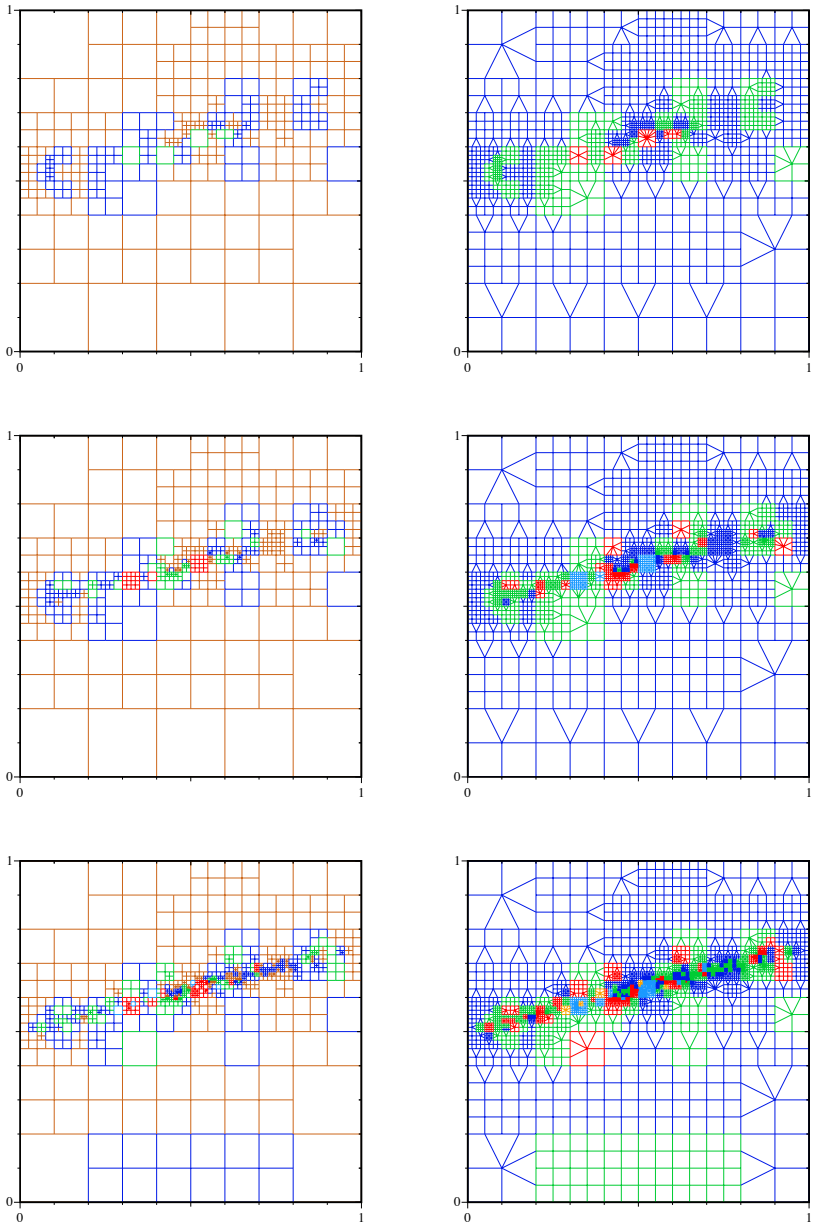

FIG. 6.31. *Test 2. Regular quadrilateral mesh; hp-refinements 9, 12, 15 on the base mesh (left) and on the reference mesh (right);* $m = 1$ *(brown),* $m = 2$ *(blue),* $m = 3$ *(green),* $m = 4$ *(red).*

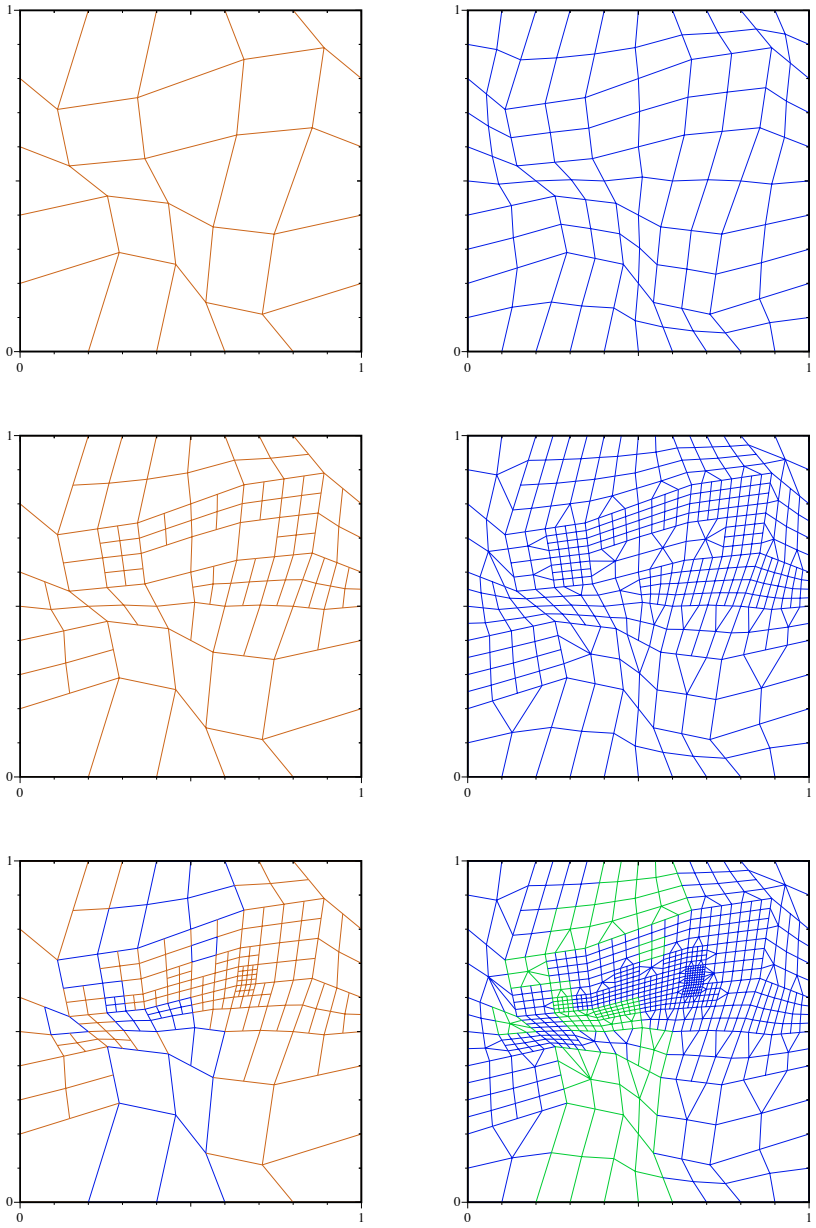

FIG. 6.32. *Test 2. Distorted quadrilateral mesh; hp-refinements 0, 3, 6 on the base mesh (left) and on the reference mesh (right);* $m = 1$ *(brown),* $m = 2$ *(blue),* $m = 3$ *(green),* $m = 4$ *(red).*

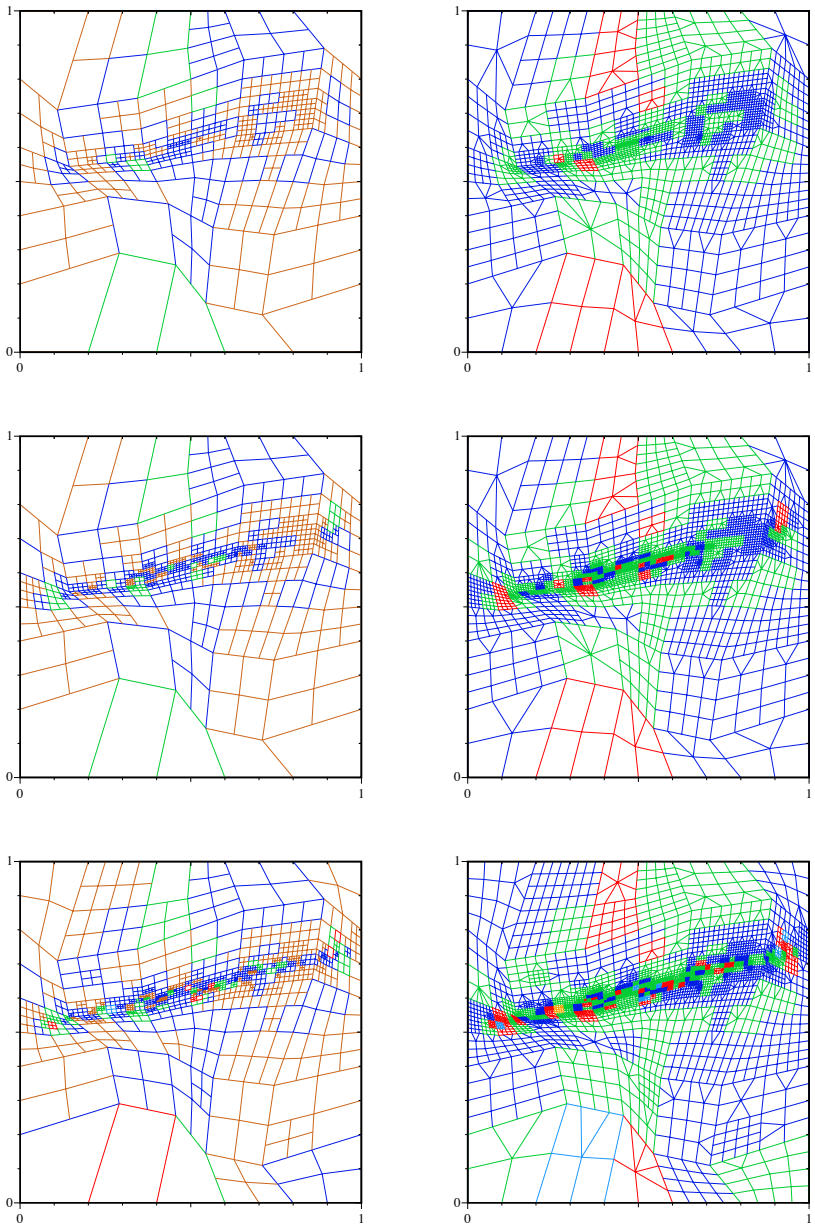

FIG. 6.33. *Test 2. Distorted quadrilateral mesh; hp-refinements 9, 12, 15 on the base mesh (left) and on the reference mesh (right);* $m = 1$ *(brown),* $m = 2$ *(blue),* $m = 3$ *(green),* $m = 4$ *(red).*